

# Distribution and female reproductive state differences in orexigenic and anorexigenic neurons in the brain of the mouth brooding African cichlid fish, *Astatotilapia burtoni*

Danielle T. Porter | David A. Roberts | Karen P. Maruska 

Department of Biological Sciences, Louisiana State University, Baton Rouge, Louisiana

## Correspondence

Karen P. Maruska, Department of Biological Sciences, 202 Life Sciences Bldg., Louisiana State University, Baton Rouge, LA 70803  
Email: kmaruska@lsu.edu

## Funding information

Support was provided by startup funds from the College of Science and Department of Biological Sciences at Louisiana State University (KPM), a Ralph E. Powe Faculty Enhancement Award from Oak Ridge Associated Universities (KPM), grants in aid of research from Sigma Xi Scientific Society and LSU Chapter of Sigma Xi (DTP), and the National Science Foundation (IOS-1456558 and IOS-1456004 to KPM).

## Abstract

Integration of reproduction and metabolism is necessary for species survival. While the neural circuits controlling energy homeostasis are well-characterized, the signals controlling the relay of nutritional information to the reproductive axis are less understood. The cichlid fish *Astatotilapia burtoni* is ideal for studying the neural regulation of feeding and reproduction because females cycle between a feeding gravid state and a period of forced starvation while they brood developing young inside their mouths. To test the hypothesis that candidate neuropeptide-containing neurons known to be involved in feeding and energy homeostasis in mammals show conserved distribution patterns, we performed immunohistochemistry and in situ hybridization to localize appetite-stimulating (neuropeptide Y, NPY; agouti-related protein, AGRP) and appetite-inhibiting (cocaine and amphetamine-regulated transcript, CART; pro-opiomelanocortin, *pomc1a*) neurons in the brain. NPY, AGRP, CART, and *pomc1a* somata showed distribution patterns similar to other teleosts, which included localization to the lateral tuberal nucleus (NLT), the putative homolog of the mammalian arcuate nucleus. Gravid females also had larger NPY and AGRP neurons in the NLT compared to brooding females, but brooding females had larger *pomc1a* neurons compared to gravid females. Hypothalamic *agrp* mRNA levels were also higher in gravid compared to brooding females. Thus, larger appetite-stimulating neurons (NPY, AGRP) likely promote feeding while females are gravid, while larger *pomc1a* neurons may act as a signal to inhibit food intake during mouth brooding. Collectively, our data suggest a potential role for NPY, AGRP, POMC, and CART in regulating energetic status in *A. burtoni* females during varying metabolic and reproductive demands.

## KEYWORDS

AGRP, CART, feeding, lateral tuberal nucleus, NPY, parental care, POMC, reproduction, teleost, RRID:AB\_2313606, RRID:AB\_2336819, RRID:AB\_2336382, RRID:AB\_514497, RRID:SCR\_014329, RRID:SCR\_014199

## 1 | INTRODUCTION

Reproduction in vertebrates is an energetically costly process, especially for females who invest in egg production and parental care (Clutton-Brock & Vincent, 1991; Grone, Carpenter, Lee, Maruska, & Fernald, 2012). Feeding and reproduction are tightly linked in most animals, and individuals must constantly sense and integrate cues from both the internal body and the external environment to make critical decisions about when to eat and when to reproduce. The brain plays a

crucial role in maintaining these motivationally driven behaviors as well as homeostatic behaviors such as food intake and body weight (Sohn, Elmquist, & Williams, 2013). Little is known, however, about which hormones and neurochemicals are involved in the complex regulation of feeding and reproduction, particularly in fishes, the largest and most diverse group of vertebrates with over 30,000 species.

Integration of reproduction and metabolism is an essential process for the survival and persistence of a species and is linked through evolutionary processes (Roa, 2013; Schneider, 2004). During reproductive

periods, energy is diverted to maintain fertility, pregnancy, and nursing (Roa, 2013; Wade & Jones, 2004). Reproduction is energetically costly, however, and during unfavorable conditions (e.g., famine, pathological conditions) the body must prioritize physiological processes essential for survival (Wade & Jones, 2004). Changes in energy stores result in the fluctuation of metabolic hormones (e.g., ghrelin, insulin, leptin), nutritional signals (e.g., glucose, lipids), and neuropeptides (e.g., Neuropeptide Y, NPY; Pro-opiomelanocortin, POMC; Agouti-related protein, AGRP; cocaine- and amphetamine-regulated transcript, CART) that regulate metabolism and fertility through interaction with the hypothalamic–pituitary–gonadal (HPG) axis (Roa, 2013; Shahjahan, Kitahashi, & Parhar, 2014). While the neural circuits controlling energy homeostasis are relatively well-characterized in mammals (Roa, 2013), the signals controlling and modulating the relay of nutritional status to the reproductive axis are not well understood in any vertebrate.

The integrative processes that regulate reproduction and metabolism are controlled by hormones and neuropeptides in the brain (Daniel, Foradori, Whitlock, & Sartin, 2013; Navarro & Kaiser, 2013; Roa, 2013; Tena-Sempere, 2007). While there are exceptions, many of the molecules that promote feeding also inhibit the reproductive system and vice versa (Schneider, 2004). For example, in mammals, feeding signals can stimulate the reproductive axis by promoting the release of gonadotropin-releasing hormone (GnRH) from the hypothalamus, and luteinizing hormone (LH) and follicle-stimulating hormone (FSH) from the pituitary to promote steroid synthesis and gamete production (Copeland, Duff, Liu, Prokop, & Londraville, 2011). However, some feeding signals, such as ghrelin (a peptide hormone typically produced by the gastrointestinal tract to stimulate hunger and feeding), inhibit the reproductive axis by suppressing the release of LH (Tena-Sempere, 2007) and the activity of the melanocortin system (Schioth & Watanobe, 2002; Tena-Sempere, 2007; Yang, Atasoy, Su, & Sternson, 2011). The melanocortin system plays an important role in the hypothalamic regulation of energy balance, and encompasses melanocyte-stimulating hormone (MSH), adrenocorticotrophic hormone (ACTH), AGRP, and the central melanocortin 3 (MC3) and 4 (MC4) receptors (Schioth & Watanobe, 2002). In teleost fishes, much like mammals, the reproductive axis is tightly connected with energy balance. For instance, the central melanocortin system in teleosts functions similarly to mammals in that up-regulation of the melanocortin receptor antagonist, AGRP, occurs during fasting in goldfish (Cerdeira-Reverter & Peter, 2003) and zebrafish (Song, Golling, Thacker, & Cone, 2003). The melanocortin system, more specifically the melanocortin 4 receptor, is also involved in the regulation of growth and reproductive hormones in zebrafish (Zhang, Forlano, & Cone, 2012). Thus, it appears that at least some of the neural control mechanisms regulating energetics and reproduction, including the melanocortin system, are conserved across vertebrates.

Metabolic status also acts to regulate the production of neuropeptides to either promote or inhibit feeding behavior (Williams & Elmquist, 2012). In mammals, the arcuate nucleus of the hypothalamus is one of the best-studied brain regions for the neural control of feeding and appetite (Sohn et al., 2013). POMC, AGRP, and NPY

neurons are all found in the arcuate nucleus and are key regulators of food intake and energy expenditure (Kong et al., 2012). Yang et al. (2011) showed that the hormone leptin is involved in a “flip-flop” memory storage circuit with ghrelin (set signal), in which leptin (reset signal) inhibits orexigenic (appetite-stimulating) neurons expressing neuropeptides such as AGRP and NPY, and stimulates anorexigenic (appetite-suppressing) neurons expressing neuropeptides such as alpha-melanocyte stimulating hormone ( $\alpha$ -MSH) and CART. POMC, NPY, AGRP, and CART are found in the lateral tuberal nucleus (NLT) of fishes, the putative homolog of the arcuate nucleus in mammals (Liu et al., 2010). Due to the structural homology of these neuropeptides across taxa (Hoskins & Volkoff, 2012), comparative studies on their distribution, function, and how they may change under varying reproductive and metabolic states in diverse taxa will contribute to our understanding of the evolution of the regulation of feeding and energy expenditure.

The African cichlid fish *Astatotilapia burtoni* is an excellent system to investigate which neuropeptides are involved in the integration of feeding and reproduction because the females cycle between an energy investment state with increased food intake to promote ovarian recrudescence and vitellogenesis, followed by spawning and a brooding maternal care state when they consume little to no food. During this brooding starvation period, which typically lasts 2 weeks in *A. burtoni*, there is a noticeable decrease in body mass and delays in ovarian cycles and subsequent spawning (Fernald & Hirata, 1979; Grone et al., 2012; Renn, Carleton, Magee, Nguyen, & Tanner, 2009). Thus, there are clear metabolic, physiological, and behavioral differences between the gravid (full of eggs) energy investment phase and the mouth brooding energy consumptive phase. Little is known, however, about potential involvement of feeding-relevant neuropeptides in the brain in regulating the cyclical transition between these divergent reproductive-energy investment states.

The purpose of this study was to test the hypothesis that the drastically different reproductive and energetic states of gravid and mouth brooding *A. burtoni* females are associated with changes in candidate orexigenic and anorexigenic neural systems. While we use the general terms orexigenic for AGRP and NPY, and anorexigenic for CART and *pomc1a*, it is important to recognize that these neuropeptides (and their respective genes) are also involved in many other functions across different brain regions. Specifically, we aimed to (1) map the distribution of candidate orexigenic (AGRP, NPY) and anorexigenic (CART) neurons in the brain for the first time in a mouth brooding fish species, and (2) quantify differences in somata sizes of AGRP-, NPY-, and *pomc1a*-expressing neurons in NLT, as well as mRNA expression levels in the hypothalamus among divergent reproductive and energetic states.

## 2 | MATERIALS AND METHODS

### 2.1 | Animals

A laboratory stock of *A. burtoni* (Günther 1894) derived from a wild-caught population originally collected from Lake Tanganyika, Africa were housed in community aquaria kept at conditions similar to their natural

environment: pH 7.8–8.0, temperature 29–30°C and a 12-hr light: 12-hr dark cycle with full spectrum illumination and constant aeration. Aquaria contained gravel along the bottom and terra cotta pot halves that served as shelters and to facilitate the establishment and maintenance of territories by dominant males. Fish were fed cichlid flakes (AquaDine, Healdsburg, CA) each morning and supplemented with brine shrimp (Sally's Frozen Brine Shrimp, San Francisco, CA) twice a week. All experiments were performed in accordance with the recommendations and guidelines stated in the National Institutes of Health (NIH) Guide for the Care and Use of Laboratory Animals, 2011. Experimental protocols were approved by the Institutional Animal Care and Use Committee (IACUC) at Louisiana State University.

To test for reproductive state differences in neuropeptide-containing neurons in the brain, we sampled both gravid females and mouth brooding parental females. Gravid females were initially selected based on body shape (distended abdomen), and gonadal status was subsequently confirmed based on oocyte diameters and gonadosomatic index (GSI) ( $GSI = [(gonad\ mass/body\ mass) * 100]$ ). Brooding females were collected 6–8 days after the onset of brooding, which is at or slightly past the mid-way point of their 12–14-day brooding period. Criteria were set for both gravid ( $GSI > 5.0$ ) and brooding ( $GSI < 1.0$ ; fry total length 5–10 mm) females to ensure that individuals within each group were of similar state. Individuals falling outside of these criteria were excluded from the dataset. Females were anesthetized in ice-cold fish tank water, sacrificed by rapid cervical transection between the hours of 8–10 am, and their body mass (BM), standard length (SL), liver mass (LM), and ovary mass (OM) were immediately measured. Once the ovaries were removed, the six largest oocytes were collected from the right ovary and the diameters of the long axis were measured and averaged. Liver mass was used to calculate the hepatosomatic index ( $HSI = [(liver\ mass/body\ mass) * 100]$ ) as a proxy for energy reserves, and ovary mass was used to calculate GSI as a measure of reproductive investment. Fulton's condition factor was also calculated using the formula  $K = 100(W/L^3)$  where  $W$  is the whole body mass in grams,  $L$  is the standard length in centimeters, and 100 is used to bring  $K$  close to 1. For brooding females, whole body mass without the presence of the brood in the buccal cavity was used to calculate  $K$ .

## 2.2 | Immunohistochemistry

Throughout this article, we use the following standard nomenclature for fishes when referring to mRNA and protein expression: lowercase and italicized names are used when referring to genes and mRNA expression measured via qPCR and in situ hybridization (ISH), while uppercase and non-italicized names are used when referring to proteins labeled by immunohistochemistry (IHC).

Following sacrifice by rapid cervical transection, brains were removed, fixed in 4% paraformaldehyde (PFA) in 1x phosphate buffered saline (PBS) overnight at 4°C, rinsed in PBS, and cryoprotected in 30% sucrose in 1xPBS at 4°C prior to sectioning. Cryoprotected brains were embedded in Optimal Cutting Temperature (OCT) compound (Tissue-Tek, Sakura Fine Tek, Torrance, CA) and sectioned in the

transverse plane at 18  $\mu$ m using a cryostat (Leica, CM1850). Sections were collected onto a series of four alternate slides (Superfrost Plus, VWR, Chicago, IL) so that all four candidate neuropeptides could be stained and analyzed in each individual brain. Additional brains used solely for peptide distribution were sectioned at 20  $\mu$ m and collected on alternate slides. Slides were dried overnight at room temperature and stored prior to staining (4°C for IHC; –80°C for ISH).

To label NPY-, AGRP-, and CART-producing neurons in the brain, we performed standard IHC. To minimize variability between individual IHC and ISH runs for quantification purposes, each staining experiment contained representatives of both gravid and brooding fish. Slides were brought to room temperature (20–22°C) and a hydrophobic barrier (Immedge pen; Vector Laboratories, Burlingame, CA) was applied around the sections and allowed to dry for about 40 min. The slides were then rinsed with 1xPBS (3  $\times$  10 min) and non-specific binding was blocked (NPY: 2 hr; AGRP, CART: 1 hr) with 1xPBS containing 0.3% Triton-X-100 (Thermo-Scientific, Pittsburgh, PA), normal goat serum (NGS; Vector Laboratories) (NPY: 8%; AGRP: 2%; CART: 8%) and bovine serum albumin (BSA; Sigma-Aldrich, Atlanta, GA) (NPY: 1.0%; AGRP: 0.2%; CART: 0.2%). Slides were then incubated with primary antibody (AGRP: 1:10,000, H-003-53, Phoenix Pharmaceuticals, Burlingame, CA; CART: 1:5,000, H-003-62, Phoenix Pharmaceuticals; NPY: 1:12,000, N9528, Sigma-Aldrich; all polyclonal made in rabbit) overnight (16–18 hr) at 4°C in a sealed humidified chamber. The primary antibody incubation was followed by 1xPBS washes (3  $\times$  10 min), incubation with a biotinylated goat anti-rabbit secondary antibody (Vector Laboratories, RRID:AB\_2313606) made in 1xPBS with NGS (NPY: 20%; AGRP: 3.3%; CART: 8.3%) for 45 min–1 hr, washes with 1xPBS (3  $\times$  10 min), quenching of endogenous peroxidases with 1.5–3.0% hydrogen peroxide in 1xPBS for 10 min, washes in 1xPBS (3  $\times$  10 min), incubation with avidin–biotin–horseradish peroxidase complex (ABC Elite kit; Vector Laboratories, RRID:AB\_2336819) (NPY: 1.5 hr; CART, AGRP: 2 hr), washes in 1xPBS (3  $\times$  10 min), and reacted with a 3,3'-diaminobenzidine (DAB) peroxidase substrate kit with nickel chloride intensification (Vector Laboratories, RRID:AB\_2336382) for 3 min. Slides were then soaked in distilled water for 10 min to stop the reaction, dehydrated in an ethanol series (50, 70, 95, 100%), cleared in xylene, and coverslipped with Cytoseal 60 mounting media (Richard-Allan Scientific, San Diego, CA).

## 2.3 | Antibody characterization

Details of the primary antibodies used in this study are provided in Table 1. All of these antibodies have been used and validated previously in other fish species [e.g., (Forlano & Cone, 2007; Sakharkar, Singru, Sarkar, & Subhedar, 2005; Singru et al., 2007)] and are listed in the JCN antibody database. The NPY polyclonal antibody (N9528; Sigma-Aldrich) was produced in rabbit using synthetic porcine NPY conjugated to keyhole limpet hemocyanin (KLH) as the immunogen, and is supplied as delipidized whole antiserum. The staining pattern in *A. burtoni* was consistent with previous localization results in other fishes (Cerdeira-Reverter et al., 2000; Gaikwad, Biju, Saha, & Subhedar, 2004; Sakharkar et al., 2005).

TABLE 1 Details of primary antibodies used in this study

Antigen	Immunogen	Host, Antibody Type, Source, Catalog #, RRID	Dilution
AGRP	Agouti-Related Protein (83–132)-NH2 (Human), immunogenic sequence: Ser-Ser-Arg-Arg-Cys-Val-Arg-Leu-His-Glu-Ser-Cys-Leu-Gly-Gln-Gln-Val-Pro-Cys-Cys-Asp-Pro-Cys-Ala-Thr-Cys-Tyr-Cys-Arg-Phe-Phe-Asn-Ala-Phe-Cys-Tyr-Cys-Arg-Lys-Leu-Gly-Thr-Ala-Met-Asn-Pro-Cys-Ser-Arg-Thr-NH2 [Contains 5 disulfide bridges. Precise positions are undetermined]	Rabbit, Polyclonal; Phoenix Pharmaceuticals #H-003-53; RRID: AB_2313908	1:10,000
CART	CART (55–102), immunogenic sequence: Ile-Pro-Ile-Tyr-Glu-Lys-Lys-Tyr-Gly-Gln-Val-Pro-Met-Cys-Asp-Ala-Gly-Glu-Gln-Cys-Ala-Val-Arg-Lys-Gly-Ala-Arg-Ile-Gly-Lys-Leu-Cys-Asp-Cys-Pro-Arg-Gly-Thr-Ser-Cys-Asn-Ser-Phe-Leu-Leu-Lys-Cys-Leu [Disulfide bonds between Cys 1-Cys 3, Cys 2-Cys 5, Cys 4-Cys 6]	Rabbit, Polyclonal; Phoenix Pharmaceuticals #H-003-62; RRID: AB_2313614	1:5,000
NPY	Synthetic NPY peptide (porcine) conjugated to KLH	Rabbit, Polyclonal; Sigma Aldrich N9528; RRID: AB_260814	1:12,000

The AGRP polyclonal antibody (H-003-53; Phoenix Pharmaceuticals, Inc.) was produced against synthetic residues 83-132 of Human AGRP and made in rabbit. Manufacturer information shows 100% cross-reactivity with AGRP (83-132)-amide (Human) and AGRP form C-NH2 (Human), and 0% cross-reactivity with Leptin, Orexin, NPY,  $\alpha$ -MSH, and CGRP. The localization pattern in *A. burtoni* was similar to that described for AGRP in zebrafish (Forlano & Cone, 2007).

The CART polyclonal antibody (H-003-62; Phoenix Pharmaceuticals, Inc.) was produced against synthetic residues 55-102 of CART (rat, mouse, bovine), and made in rabbit. Manufacturer information shows Western blot detection of a 5-kDa band in rat brain and 100% cross-reactivity with CART 55-102 (rat, mouse, bovine, and human), 71.8% cross-reactivity with CART 61-102 (human), 0.01% cross-reactivity with AGRP 83-132-NH2 (human), and 0% cross-reactivity with Leptin, NPY,  $\alpha$ -MSH, Orexin, and MCH. The staining pattern in *A. burtoni* was consistent with previous localization results in zebrafish (Akash, Kaniganti, Tiwari, Subhedar, & Ghose, 2014; Mukherjee, Subhedar, & Ghose, 2012).

To test for antibody specificity in the cichlid brain tissue, we performed two different types of controls. First, we preabsorbed each antibody (anti-NPY, -AGRP, -CART) with its respective immunizing control peptide (NPY: 1.617  $\mu$ M, Sigma-Aldrich, #N5017; CART 55–102 peptide fragment: 1.521  $\mu$ M, Phoenix Pharmaceuticals, #003-62; AGRP 83-132 peptide fragment: 706.6 nM Phoenix Pharmaceuticals, #003-53) in excess overnight at 4°C prior to tissue application. These preabsorption controls eliminated all reaction products and resulted in no staining when run simultaneously with non-preabsorbed antibody (Figure 1). Other procedural controls (omission of secondary antibody, ABC, and DAB) also resulted in no staining. Second, we performed ISH to label mRNA for *agrp* ( $N = 2$ ,  $SL = 45.1 \pm 1.50$  mm,  $BM = 2.94 \pm 0.93$  g,  $GSI = 0.85 \pm 1.43$ ), *npy* ( $N = 5$ ,  $SL = 38.2 \pm 1.92$  mm,  $BM = 1.61 \pm 0.26$  g,  $GSI = 1.14 \pm 0.98$ ), *cart2* ( $N = 7$ ,  $SL = 39.0 \pm 6.4$  mm,  $BM = 1.91 \pm 0.64$  g,  $GSI = 2.19 \pm 2.38$ ) and *cart4* ( $N = 4$ ,  $SL = 39.3 \pm 6.8$  mm,  $BM = 1.86 \pm 0.44$  g,  $GSI = 3.13 \pm 2.62$ ) (described below) on females of mixed reproductive states (Figures 1, 2). We used ISH rather than western blots to more accurately compare

it to the localization of different IHC-identified cell populations within sectioned brain tissue.

Staining of *agrp* mRNA in cells of the NLT was identical to that observed by AGRP antibody (Figure 2a,b). However, the AGRP antibody also stained the large neurons of gTN, which were not labeled via ISH. This IHC label remained after preabsorption of the AGRP antibody with excess AGRP peptide, suggesting that it is cross-reactive binding to some non-AGRP substance, similar to that described in the zebrafish (Forlano & Cone, 2007).

For *npy*, while mRNA was primarily localized to all of the same regions labeled with the NPY antibody (Figure 2c,d) (with the exception of weak to no label in DT and gTN neurons with ISH, but strong antibody label), there were also numerous additional cells labeled throughout the brain by ISH that were not detected by the antibody (e.g., ICL, Vs, PGZ, IO, SGn, SVn). Duplicate *npy* genes (*npya*, *npyb*) are identified in *A. burtoni* (Hu et al., 2016), and our *npy* ISH results likely represent the distribution of *npya*. We chose to examine this form rather than the teleost-specific duplicate, *npyb*, because in the related Nile tilapia *O. niloticus*, *npya* is expressed at much higher levels in the brain compared to *npyb*, responds to changes in feeding conditions that are not evident in *npyb*, and intracranial injections stimulate food intake (Yan et al., 2017). Thus it is possible that the neurons labeled in DT and gTN with IHC in *A. burtoni* represent *npyb* populations.

Similarly, the cells labeled by the CART antibody were primarily localized to the same regions as either *cart2* or *cart4* mRNA, but there were also additional *cart2* and *cart4* cells not detected by the CART antibody, and a population of large midline cells in nMLF that stained with the antibody but not *cart2* or *cart4* ISH (Figure 2e-h). Six CART prohormones are identified in *A. burtoni* (Hu et al., 2016), and we chose to examine *cart2* and *cart4* because of their known roles in feeding and energy metabolism, and their widespread localization in the brain of zebrafish, including hypothalamic regions involved in metabolic regulation such as NLT (Akash et al., 2014).

Some possibilities for the differences in staining between IHC and ISH include variations in protein translation (i.e., turnover, or post-



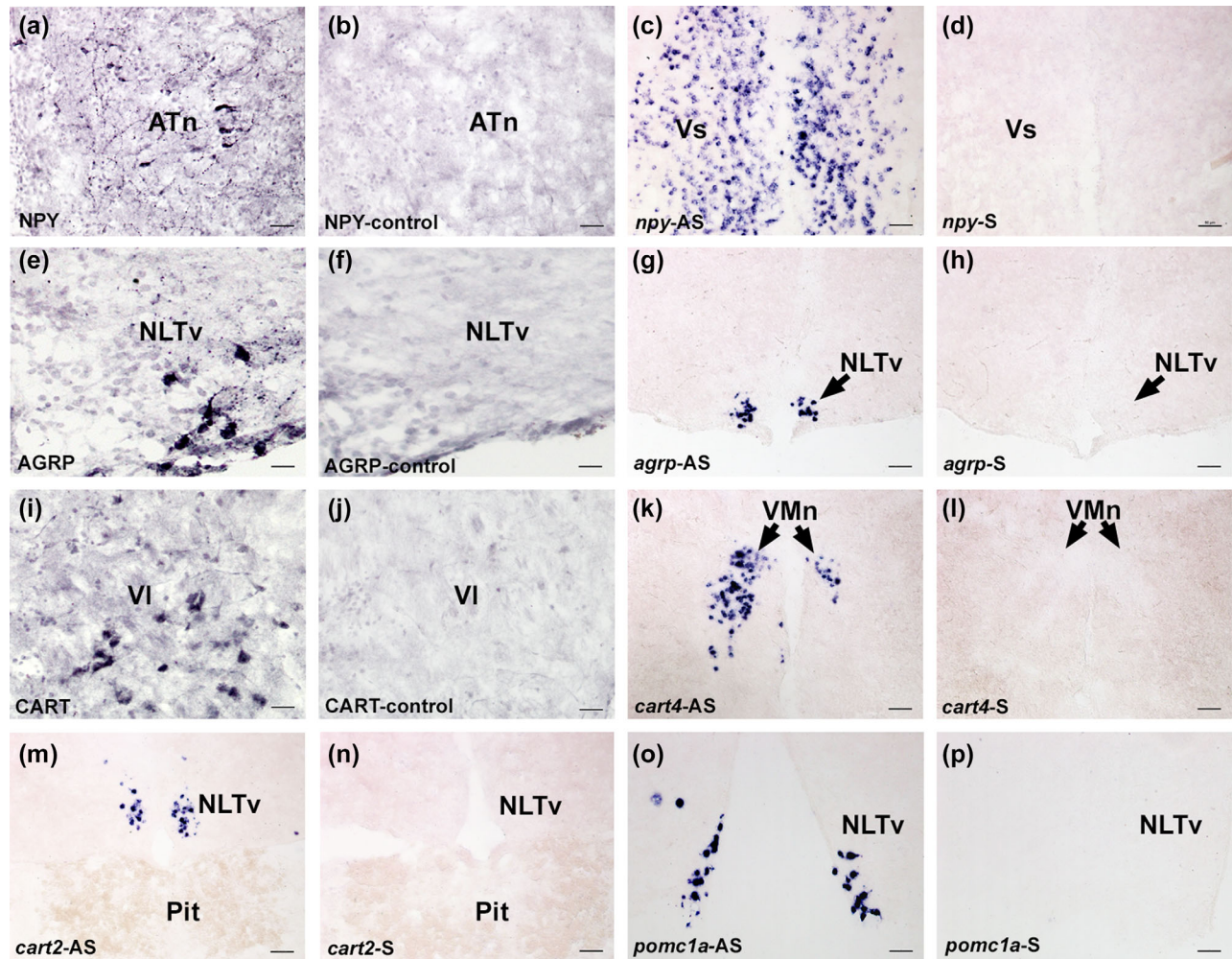


**FIGURE 1** Photomicrographs showing antibody specificity for NPY, AGRP and CART, and specificity of probe binding for *npy*, *agrp*, *cart2*, *cart4*, and *pomc1a* in the brain of *A. burtoni* females. Representative coronal sections showing typical positive staining along with adjacent control alternate sections stained with preabsorbed antibody (IHC) or sense probes (ISH) for NPY IHC (a, b), *npy* ISH (c, d), AGRP IHC (e, f), *agrp* ISH (g, h), CART IHC (i, j), *cart4* ISH (k, l), *cart2* ISH (m, n) and *pomc1a* ISH (o, p). S, sense; AS, anti-sense. Scale bars = 25  $\mu$ m in (a, b), (e, f), and (i, j); 50  $\mu$ m in (c, d), (g, h), (k, l), (m, n), (o, p). See list for abbreviations. [Color figure can be viewed at [wileyonlinelibrary.com](http://wileyonlinelibrary.com)]

translational modifications), low levels of protein or mRNA not detected by each staining technique, binding characteristics between antigens and antibodies/probes, differences between mRNA transcription and peptide storage within cells, cross-reactivity of antibodies with related peptides, or labeling of different gene forms due to teleost whole genome duplication.

## 2.4 | Synthesis of riboprobes for ISH

To identify *pomc1a*, *agrp*, *npy*, *cart2*, and *cart4* mRNA-containing neurons, we performed chromogenic-based ISH. To identify *pomc1a*-containing neurons, we performed ISH as a proxy for  $\alpha$ -MSH. This approach was used because pilot experiments with several commercially available  $\alpha$ -MSH antibodies failed to produce reliable staining. Following the teleost-specific whole genome duplication, three forms of *pomc* (*pomc1a*, *pomc1b*, and *pomc2*) are identified in *A. burtoni* and their localization in the brain and pituitary

of this species was previously described (Harris, Dijkstra, & Hofmann, 2014; Hu et al., 2016). We chose to quantify *pomc1a* neurons because phylogenetic analyses indicate that *pomc1a* is the homolog to the mammalian form responsible for the synthesis and cleavage of  $\alpha$ -MSH in the pituitary in response to satiety signals (Amano et al., 2005).

To localize cells, we used a digoxigenin (DIG) ISH protocol with riboprobes. Primers for each candidate gene were designed from the *A. burtoni* sequences available in Genbank (Table 2) and then commercially synthesized (Life Technologies, Bethesda, MD). Templates for the riboprobes were generated by PCR (PCR Platinum SuperMix, Life Technologies) from whole brain *A. burtoni* cDNA using gene-specific primers. The reaction conditions were as follows: 95°C for 1 min, 40 cycles of: (95°C for 15 s, 55°C for 15s, 72°C for 1 min), and 72°C for 1 min. Purified PCR products (MinElute PCR kit, Qiagen, Chatsworth, CA) were then used as the template in the transcription reaction to incorporate DIG-labeled nucleotides (DIG RNA-labeling mix, Roche,

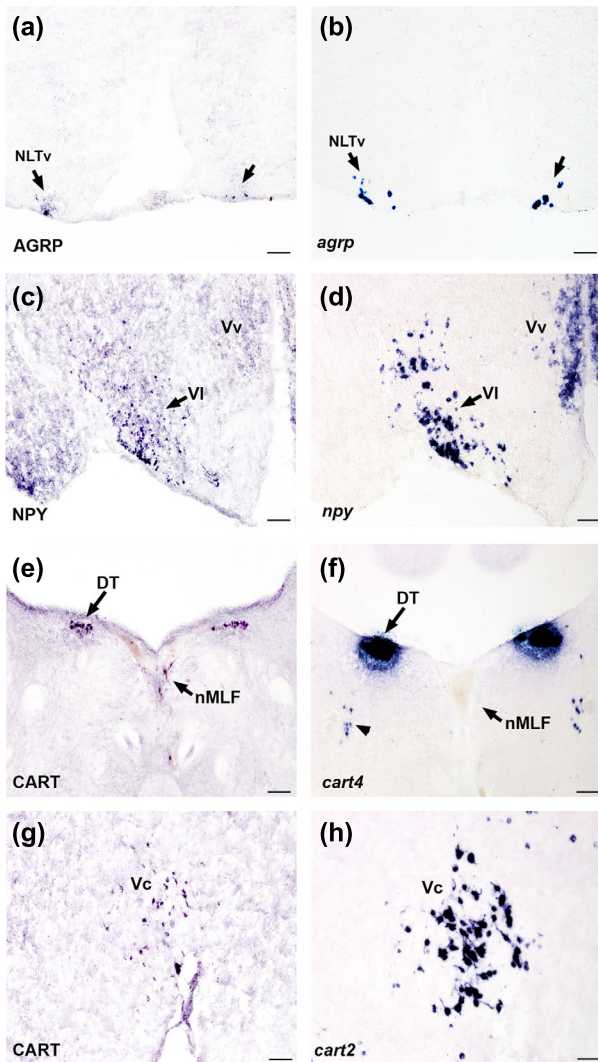


**FIGURE 2** Representative photomicrographs of alternate sections stained via immunohistochemistry (IHC) and *in situ* hybridization (ISH) for candidate neuropeptides in the brain of *A. burtoni*. AGRP antibody (a) and *agrp* ISH probe (b) both label cells in the NLTv (arrows). NPY antibody labels cells in VI, but only shows fibers in Vv (c). *npy* ISH shows labeled cells in VI similar to the antibody, but also reveals *npy*-expressing cells in Vv (d), as well as many other regions (see Methods and Results). The CART antibody labels large cells in DT (e), which are also detected via *cart4* ISH (f). However, the CART antibody also labels large neurons in nMLF along the midline, which are not detected by *cart4* ISH. An additional small cell population consistently observed in the tegmentum also contains *cart4*-expressing cells (arrowhead) that is not detected by the antibody. CART antibody also labels cells in Vc (g), which are also detected with *cart2* ISH (h). Scale bars = 50  $\mu$ m (a–d, g, h) and 100  $\mu$ m (e, f). [Color figure can be viewed at [wileyonlinelibrary.com](http://wileyonlinelibrary.com)]

Nutley, NJ) into the nucleic acid sequence, followed by probe purification (GE Illustra Probe Quant G-50 microcolumns). Probes were transcribed from the T3 polymerase transcription initiation sequence (aattaaccctcactaaaggg) that was added to the reverse (for anti-sense probes) or forward (for sense control probes) gene-specific primers. PCR products and final probes were checked on a 1% agarose gel and

verified to be bands of the correct size. Probes were diluted with hybridization buffer and stored at  $-20^{\circ}\text{C}$ .

## 2.5 | In situ hybridization

Chromogenic-based ISH was performed as previously described (Butler & Maruska, 2016; Grone & Maruska, 2015; Maruska, Butler, Field, & Porter, 2017), and all solutions used during the protocol were RNase-free (0.25  $\mu$ m filtered). Briefly, sections were brought to room temperature ( $20$ – $22^{\circ}\text{C}$ ) and a hydrophobic barrier (Immedge pen, Vector Laboratories) was applied and allowed to dry for about 40 min. The slides were then washed in 1xPBS ( $3 \times 5$  min), fixed in 4% PFA (20 min), washed in 1xPBS ( $2 \times 5$  min), permeabilized in proteinase K (10  $\mu$ g/ml final concentration, 10 min), washed in 1xPBS (10 min), fixed in 4% PFA for 15 min, washed in 1xPBS ( $2 \times 5$  min), rinsed in milliQ water (3 min), incubated in 0.1M triethanolamine-HCl (pH 8.0) with acetic anhydride to 0.25% volume (10 min), washed in 1xPBS (5 min), and incubated for 2.5 hr in pre-hybridization buffer at  $60$ – $65^{\circ}\text{C}$  in a sealed humidified chamber. The pre-hybridization solution was removed, DIG-labeled anti-sense probe was added (sense probes with the T3 sequence added to the forward primer were also used as controls to test probe specificity; Figure 1), and slides were covered with hybridization solution to hybridize overnight (12–16 hr) at  $60$ – $65^{\circ}\text{C}$  in a sealed humidified chamber. Following hybridization, the slides were washed at  $60$ – $65^{\circ}\text{C}$  in pre-warmed 2X saline-sodium-citrate (SSC):50% formamide ( $2 \times 30$  min), 1:1 mixture of 2XSSC: Maleic acid buffer with 0.1% Tween-20 (MABT) ( $2 \times 15$  min), and MABT ( $2 \times 10$  min). Slides were then washed at room temperature with MABT ( $2 \times 10$  min) and non-specific binding was blocked with MABT containing 2% BSA for 3 hr. Slides were then incubated with alkaline phosphatase-conjugated anti-DIG Fab fragments (Roche, RRID: AB\_514497) diluted 1:5,000 in blocking solution (MABT with 2% BSA) at  $4^{\circ}\text{C}$  overnight in a humidified chamber. Slides were then washed with MABT ( $3 \times 30$  min) at room temperature, incubated in alkaline phosphatase (AP) buffer ( $2 \times 5$  min), developed for 2–5 hr with 4-nitro-blue tetrazolium chloride/5-bromo-4-chloro-3-indolyl-phosphate (NBT/BCIP, Roche) substrate solution at  $37^{\circ}\text{C}$ . Slides were then washed with 1xPBS ( $3 \times 5$  min) to stop the reaction, fixed in 4% PFA (10 min), washed in 1xPBS ( $3 \times 5$  min), and coverslipped with aqueous mounting media (Aqua-mount, Thermo-Scientific).

## 2.6 | Quantification of somata size

To test for reproductive state differences in neuropeptide-expressing neurons, we performed blind unbiased measurements of somata sizes for NPY, AGRP, and *pomc1a* labeled neurons from transverse sections without knowledge of the SL, BM, GSI or reproductive state of the fish. Cell size was determined by measuring cell profile areas contained within NLTv, NLTi, and NLTm (Figure 3a–d) from 10 randomly selected neurons for NPY (representing 24% of all cells) and AGRP (22% of cells), and 20 randomly selected neurons for *pomc1a* (25% of cells) per individual. We did not measure CART-ir somata because we could not



TABLE 2 Primer sequences used for qPCR and to generate templates for synthesis of riboprobes for in situ hybridization

Gene	Forward (5'→3')	Reverse (5'→3')
Primer Sequences for qPCR		
<i>pomc1a</i>	ACAGATCCAATCAGCCTTTCC	GACCACTCTCTTTCCCTTTG
<i>npy</i>	CCTTGACGGAGGCATACCC	GAGGTTGATGTAATGTCTCAGC
<i>agrp</i>	GGATTCTGGTCTGCTAAA	CATCGAGCATTCCGGTGAA
<i>cart2</i>	CCCACCCACTTTATGTCACTAG	CTGAGACTTTACAGCGTGTATG
<i>cart4</i>	CAATCGTCTCGTCCATATT	CCGTGCAGCTTTATGAAGAA
<i>lepr</i>	CGGGAGAAGGACTTGTATTATC	GCTCCACTTTGGCTTCTT
<i>ghs-r1</i>	CGTGTCTCACAGGGATAAGA	TAGCGACCCACATGGAAG
Primer Sequences for Riboprobes <sup>a</sup>		
<i>pomc1a</i>	GGCAGGTGCAGATGCACACAGAGAATG	AGCTTTCATGACCCCGCCGTAAC
<i>npy</i>	CAAGCGCTCAGAAGAGAAA	CACAGATGACGACTCAGAATAA
<i>agrp</i>	CACTGAAACCTCCTCTATC	GCACAATCCACACATAGATTTT
<i>cart2</i>	GTGGAGCGACTTTTGAGAC	TCGCCACCATCCTTACA
<i>cart4</i>	CAGACACCACAGAAGAAGAC	GAGCCGTGCAGCTTTAT

<sup>a</sup>T3 transcription initiation sequence (aattaacctactaaaggg) was added to the reverse primer (for antisense probes) or forward primer (for sense control probes) for riboprobes.

always identify clearly distinguishable cells in the NLT, primarily due to the proximity of these cells to the brain edge, which made it difficult to accurately measure cell areas due to tissue folding, edge-effect staining, and accumulation of debris during staining protocols. Measurements were taken at a point where the labeled cell perimeter was easily discernible and a distinct nucleus was visible under the 40× objective lens. Somata areas for each neuropeptide-containing cell type were then averaged for each individual and within each reproductive state (gravid and mouth brooding) for statistical comparisons.

## 2.7 | Imaging and analysis

To map the distribution patterns for neuropeptide-containing neurons in the brain, stained slides were visualized on a Nikon Eclipse Ni microscope and photographs were taken with a color digital camera (Nikon DS-Fi2) controlled by Nikon elements software (RRID:SCR\_014329). Neuroanatomical regions and specific brain nuclei were identified using atlases and cytoarchitecture previously described in *A. burtoni* (Burmeister, Munshi, & Fernald, 2009; Maruska et al., 2017; Munchrath & Hofmann, 2010) as well as in other fish species (Imura et al., 2003; Munoz-Cueto, Sarasquete, Zohar, & Kah, 2001; Wullimann, Rupp, & Reichert, 1996). Images were sharpened, adjusted for contrast, brightness, and levels, and distracting artifacts removed with the clone tool in Photoshop CS6 (Adobe Systems, San Jose, CA.; RRID:SCR\_014199). Neuropeptide distribution maps were created by tracing the outline of the left side of a representative cresyl-violet-stained coronal section along with relevant nuclei and neuroanatomical structures. The traces were then duplicated and flipped horizontally to create a mirror image for representation of a full coronal section, and then the locations of immunoreactive cells and fibers for each neuropeptide were marked on top of the coronal section. Cells were defined as stated above and immunoreactive fiber densities were defined as follows: few = 4 or less, low density = greater than 4 but less than 20, moderately

dense = 21–45, and dense = greater than 45 in the field of view using a 40× objective lens.

## 2.8 | Quantitative PCR (qPCR)

To examine the mRNA levels of the same neuropeptides quantified for somata size and distribution, as well as several other relevant genes, we performed qPCR on macro-dissected hypothalamic regions from a different set of females. Gravid ( $N = 15$ ) and mouth brooding ( $N = 13$ ) females were sacrificed as described above and the brains were macro-dissected to first divide the brain into the telencephalon, diencephalon and mesencephalon, and rhombencephalon (Figure 3e). The diencephalon was then further dissected so that the hypothalamus (without pituitary gland) was removed and used for qPCR. The brain was macro-dissected in this fashion to focus on the NLT, where somata sizes were quantified in a different set of animals, but also included other diencephalic nuclei (e.g., ATn, NRL, NDIL, NRP, NCIL) known to be involved in feeding and reproduction. This approach also removed any NPY, AGRP, CART, and/or *pomc1a* populations in other brain regions such as the preoptic nuclei. The hypothalamic tissue was weighed (2–6 mg per individual), rapidly frozen on dry ice, and then immediately stored at  $-80^{\circ}\text{C}$  until RNA isolations were performed.

Hypothalamic tissue was homogenized and total RNA was extracted following manufacturer's protocols (RNeasy Mini Plus Kit, Qiagen). RNA yields were calculated using spectrophotometric values to ensure that a consistent amount of RNA (250 ng/ $\mu\text{l}$ ) was used as a template for cDNA synthesis (iScript, Bio-Rad, Hercules, CA). The resulting cDNA was then re-measured via spectrophotometry to check the quality, and then diluted 1:5 prior to qPCR. Primers for all genes of interest [*pomc1a*, *agrp*, *ghrelin receptor (ghs-r1)*, *leptin receptor (lepr)*, *cart2*, *cart4*, *npy*] were designed from *A. burtoni* sequences available in Genbank (Table 2) using PrimerQuest (Integrated DNA Technologies, Coralville, IA) and then commercially synthesized (Life Technologies). qPCR was performed on a CFX connect Real-Time system (Bio-Rad) with duplicate reaction volumes of 20  $\mu\text{L}$ . Reaction parameters were as follows: 95°C for 30 s, 45 cycles of 95°C for 1 s and 60°C for 30 s, and

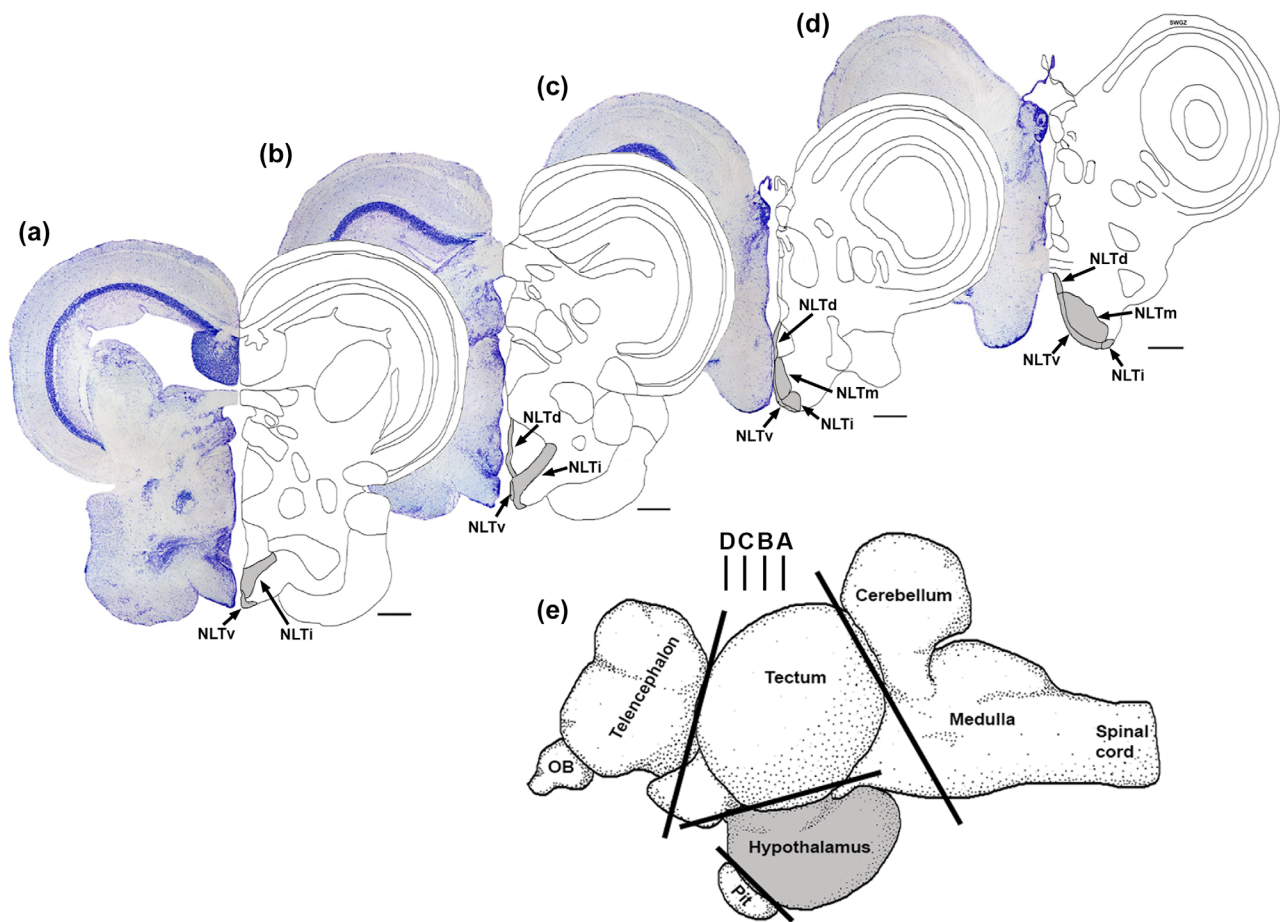


**FIGURE 3** Brain regions used for somata size measurements and qPCR. Caudal (a) to rostral (d) transverse sections showing NLT regions (NLTd, NLTi, NLTm, NLTv; shaded gray) of the hypothalamus. Somata size measurements were taken for *AGRP*, *NPY*, and *pomc1a* from the NLTv, NLTi, and NLTm throughout the rostro-caudal extent shown. Left side shows cresyl violet stained section and right side shows traced nuclei. Scale bars (a–d) = 250  $\mu$ m. Approximate location of each transverse section is indicated on (e). Hypothalamic tissue (shaded gray in e) used for qPCR analysis was macro-dissected via cuts (lines) at the locations indicated on the sagittal brain illustration shown in (e). See list for abbreviations. [Color figure can be viewed at [wileyonlinelibrary.com](http://wileyonlinelibrary.com)]

65°C for 5 s, followed by a melt curve analysis. Fluorescence thresholds for each sample were automatically measured (CFX Manager, BioRad) and then PCR Miner (Zhao & Fernald, 2005) was used to calculate cycle thresholds and reaction efficiencies for individual wells as described previously (Maruska, Becker, Neboori, & Fernald, 2013; Maruska, Levavi-Sivan, Biran, & Fernald, 2011; Maruska, Zhang, Neboori, & Fernald, 2013). This curve-fitting qPCR algorithm objectively calculates reaction efficiency and the fractional cycle number at threshold (CT) of the amplification curve for more accurate computation of mRNA levels. The relative amount of mRNA was then normalized to the geometric mean of the two reference genes *18s* rRNA and *rpl32* (60S ribosomal protein L32) using the following equation: relative target mRNA levels =  $[1/(1 + E_{\text{target}})^{\text{CT}_{\text{target}}}] / [1/(1 + E_{\text{geomean}})^{\text{CT}_{\text{geomean}}}] \times 100$ , where  $E$  is the reaction efficiency and CT is the average cycle threshold of the duplicate reactions. Values of *18s* (Mann–Whitney;  $U = 73.00$ ;  $p = 0.421$ ) and *rpl32* (student's  $t$  test;  $p = 0.939$ ;  $t = 0.0771$ ;  $df = 25$ ) did not differ between gravid and brooding females, indicating they are appropriate reference genes for this study. Normalizing the mRNA levels to two reference genes, rather than one, allows for a more accurate quantification (Bustin, Benes, Nolan, & Pfaffl, 2005; Mitter et al., 2009).

## 2.9 | Statistical analyses

To test for differences between reproductive states in physiological variables (GSI, HSI, oocyte diameter, SL, BM) we used two-tailed unpaired  $t$  tests or non-parametric Mann–Whitney tests when assumptions of normality and equal variance were not met (SigmaPlot, Systat, Inc., San Jose, CA). Pearson Product Moment Correlations were used to test for correlations between GSI and somata sizes (compared between each peptide), HSI and somata sizes, and between different somata sizes. To account for positive relationships between somata size and body size, we compared gravid and brooding somata sizes with analysis of covariance (ANCOVA), using standard length (for somata size comparisons) or hypothalamic mass (for mRNA level comparisons) as a covariate. Statistical significance was set at  $p = 0.05$  for all comparisons. Bonferroni corrections or other similar procedures for multiple testing were not used because they reduce statistical power and increase the chance of type II errors, especially in small sample sizes. While these correction tests do reduce type I errors, their unacceptable effects on statistical power can mask potential biologically relevant results and interpretations (Nakagawa, 2004).

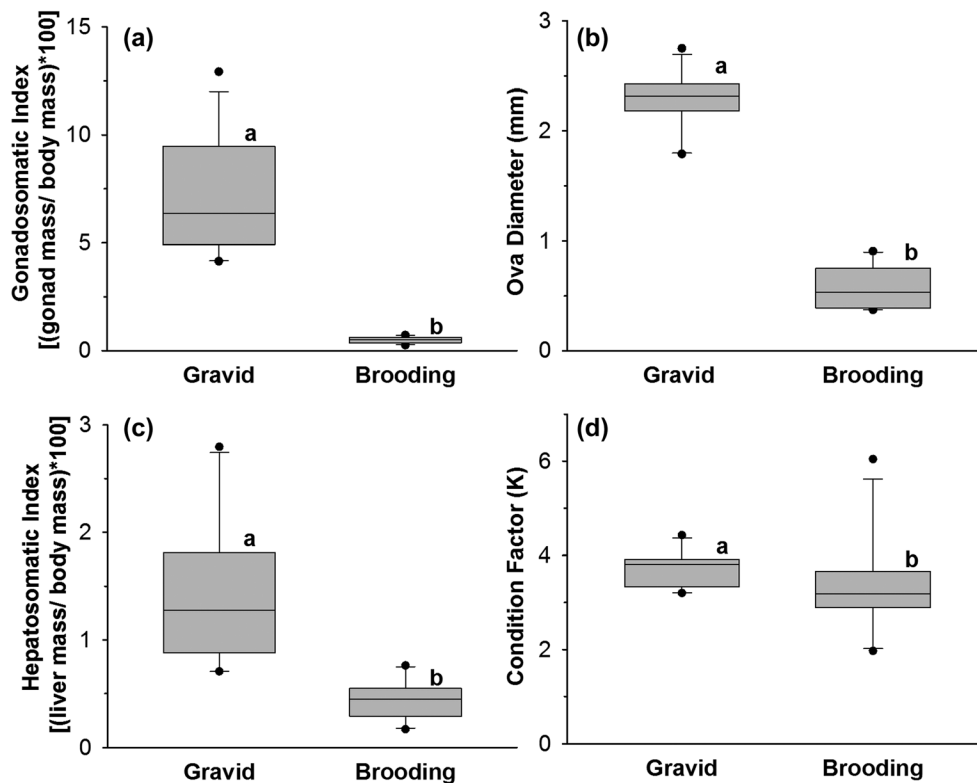


**FIGURE 4** Physiological differences between gravid and mouth brooding *A. burtoni* females. Gravid females have greater gonadosomatic index (GSI) (a), ova diameters (b), hepatosomatic index (HSI) (c), and condition factors (d) compared to brooding females. In each graph, the bottom of each box is the 25th percentile, the top is the 75th percentile and the line in the middle is the median. Whiskers (error bars) indicate the 10th and 90th percentiles and dots represent points outside the 10th–90th percentile.  $N = 12$  for both gravid and brooding females for (a–d). Different letters indicate statistical differences at  $p < 0.05$

### 3 | RESULTS

#### 3.1 | Physiological differences between gravid and brooding females

A total of 24 female *A. burtoni* (12 gravid, 12 brooding) were used in this study for the physiological analysis, quantification of somata sizes, and IHC distribution of neuropeptides. Gravid females have higher GSI (Mann–Whitney;  $U = 0.00$ ;  $p < 0.001$ ) (Figure 4a) and larger ova diameters (Student's  $t$  test;  $p < 0.001$ ;  $t = 17.614$ ;  $df = 22$ ) (Figure 4b) compared to brooding females. Gravid females also have higher HSI (Mann–Whitney;  $U = 4.00$ ;  $p < 0.001$ ) (Figure 4c) and condition factors (Mann–Whitney;  $U = 25.00$ ;  $p = 0.013$ ) (Figure 4d) compared to brooding females, indicative of greater energy reserves.

#### 3.2 | Distribution of NPY, AGRP and CART neurons

##### 3.2.1 | Localization of NPY-immunoreactivity

###### Olfactory bulbs and telencephalon

NPY-ir cells occur in the ganglion of the terminal nerve (gTN) at the junction between the olfactory bulbs and rostral telencephalon (Figures 5, 6a). In the olfactory bulbs, NPY-immunoreactive (-ir) fibers are present in the external cell layer (ECL), glomerular layer (GL), inner cell layer (ICL) and secondary olfactory layer (SOF) (Figure 5a).

NPY-ir cells are essentially absent from dorsal telencephalic nuclei, with the exception of a few scattered cells in some regions of the central part of the dorsal telencephalon (Dc) (Figures 5d, 6b). NPY-ir cells lie in several nuclei of the ventral telencephalon, including the lateral part of the ventral telencephalon (Vl) (Figures 5b–d, 6c), rostral portion of the central part of the ventral telencephalon (Vc) (Figures 5b, c, 6c), ventral nucleus of the ventral telencephalon (Vv) (Figure 5b), and a few small cells in the rostral subdivision of the dorsal part of the ventral telencephalon (Vd-r) (Figure 5c).

NPY-ir fibers are abundant throughout the dorsal telencephalic regions (Figure 5a–f). Low to moderately dense scattered NPY-ir fibers are present in the ventral part of the lateral zone of the dorsal telencephalon, subdivision 1 (DI-v1), dorsal part of the lateral zone of the dorsal telencephalon (DI-d), and medial part of the dorsal telencephalon, subdivision 1 (Dm-1) (Figure 5a–c). Moderately dense NPY-ir fibers are present in the rostral ventral region of the lateral part of the dorsal telencephalon, subdivision 2 (DI-v2) and density increased caudally in the DI-v2 (Figure 5b–d). Dense fibers lie in the nucleus taenia (NT) (Figure 5d) and dorsal part of the dorsal telencephalon (Dd) (Figure 5d–f). Dense fibers are also present in rostral sections of the ventral area of the central part of the dorsal telencephalon, subdivision 1 (Dc-1). In more caudal regions of Dc-1, fibers remain dense in the medial area, while fiber density decreases to moderate levels in the lateral area of Dc-1 (Figure 5b, c). Moderately dense fibers are present in the



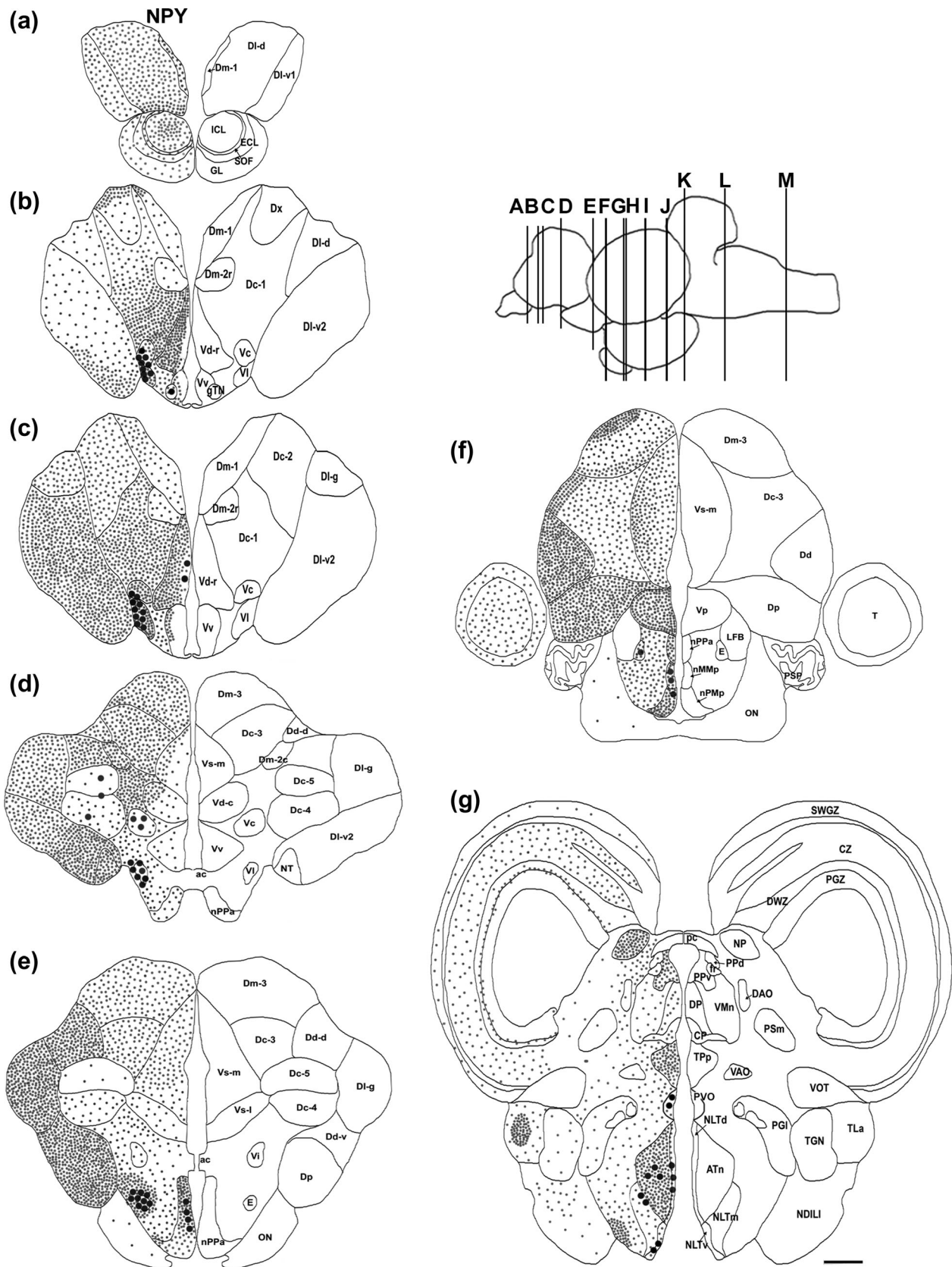


**FIGURE 5** Localization of neuropeptide Y (NPY)-immunoreactive neurons in the brain of *A. burtoni*. Representative line drawings of transverse sections from rostral (a) to caudal (n) brain regions show the locations of NPY ir-somata (large black dots) and fibers (small black dots). Left side of brain shows NPY distribution and right side shows labels of nuclei and other neuroanatomical structures. Figure inset at the top right shows a lateral view of the brain indicating the approximate location of each transverse section. Scale bar = 250  $\mu$ m. See list for abbreviations

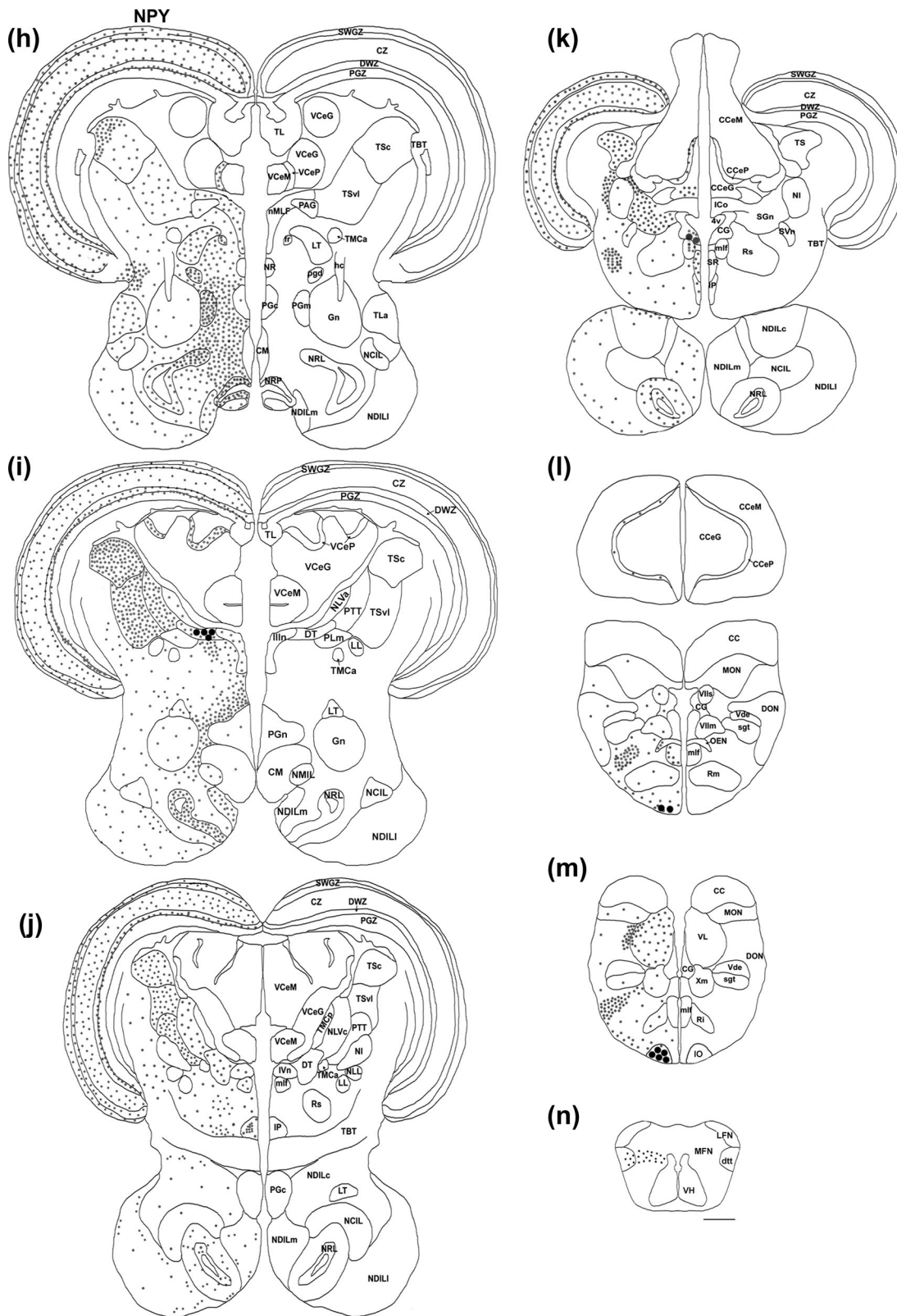
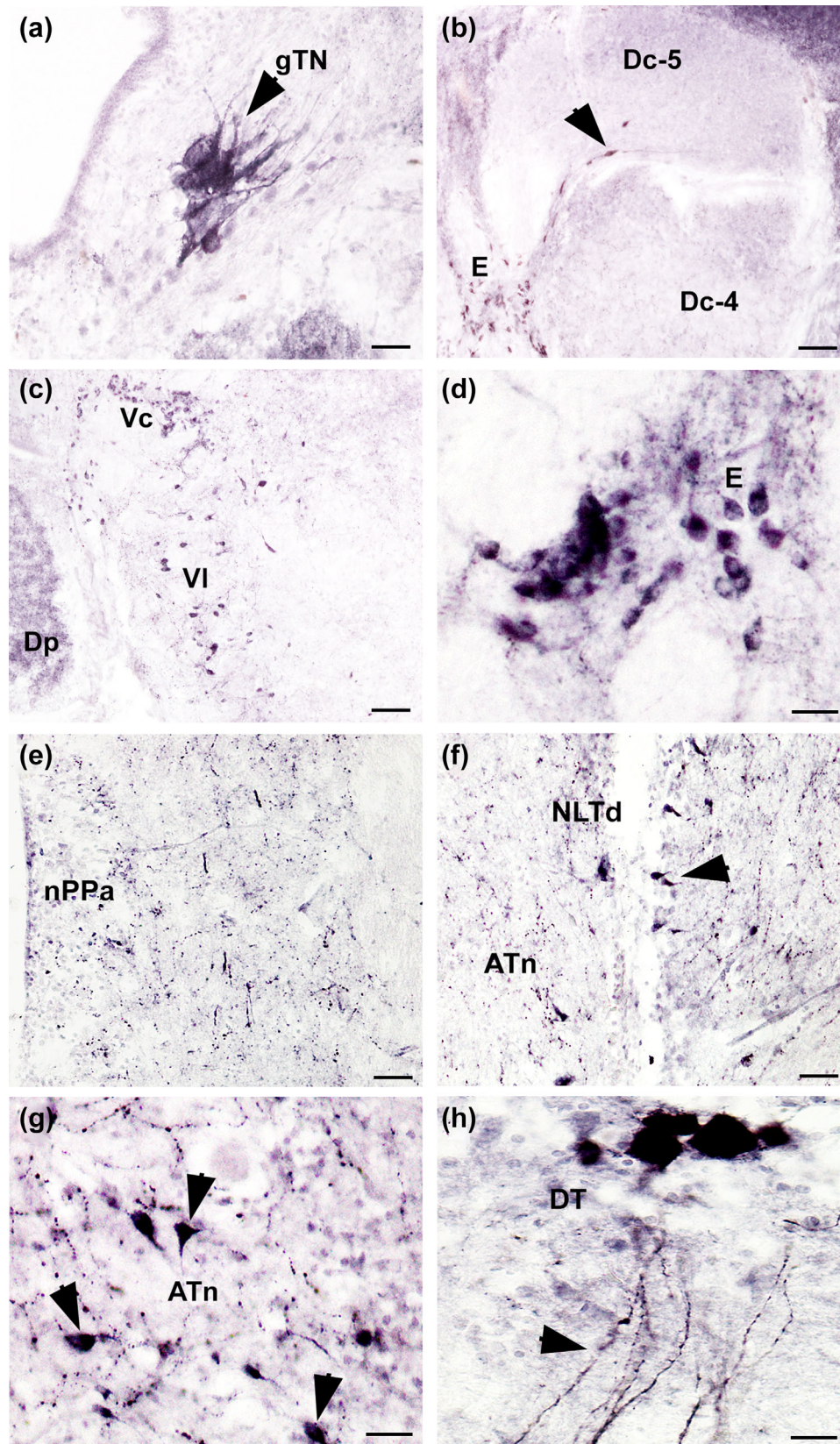


FIGURE 5 (Continued)

unassigned subdivision of the dorsal telencephalon (Dx) (Figure 5b), dorsal part of the dorsal telencephalon, dorsal subdivision (Dd-d) (Figure 5d, e), medial part of the dorsal telencephalon, caudal subdivision 2

(Dm-2c) (Figure 5d), medial part of the dorsal telencephalon, subdivision 3 (Dm-3) (Figure 5d-f), central part of the dorsal telencephalon, subdivision 3 (Dc-3) (Figure 5d-f), and granular zone of the lateral part





**FIGURE 6** Representative photomicrographs of NPY-immunoreactive somata and fibers in the brain of *A. burtoni*. Coronal sections showing NPY-ir cells in gTN (a). NPY-ir cells in the region between Dc-4 and Dc-5 (arrowhead) (b). Cells and fibers in the Vc and VI (c) and entopeduncular nucleus (d). NPY-ir fibers in the nPPa (e). In the diencephalon, NPY-ir cells and fibers are found in the ATn and NLTd of the hypothalamus (arrowheads) (f, g). Large NPY-ir cells in DT and ventrally projecting varicose fibers (arrowhead) (h). Scale bars = 50  $\mu$ m (b, c); 25  $\mu$ m in (a), (e), (f); 10  $\mu$ m in (d), (g), (h). See list for abbreviations. [Color figure can be viewed at [wileyonlinelibrary.com](http://wileyonlinelibrary.com)]

of the dorsal telencephalon (DI-g) (Figure 5c–e). Low density fibers also lie in the medial part of the dorsal telencephalon, rostral subdivision 2 (Dm-2r) and central part of the dorsal telencephalon, subdivisions 4 (Dc-4) and 5 (Dc-5) (Figure 5d, e).

Compared to dorsal telencephalic nuclei, NPY-immunoreactive fibers are less dense in ventral telencephalic nuclei, particularly the periventricular regions along the midline (Figure 5b–f). Moderately dense NPY-ir fibers are present in the VI (Figure 5b–d), medial part of the supracommissural nucleus of the ventral telencephalon (Vs-m) (Figure 5d–f), Vv (Figure 5b, c), Vc (Figure 5b, c), and in the Vd-r. Fiber density increases in the Vd-r from moderately dense in rostral sections to dense in more caudal regions (Figure 5b, c). The postcommissural nucleus of the ventral telencephalon (Vp) and intermediate nucleus of the ventral telencephalon (Vi) contain moderately dense to dense fibers, and the lateral part of the supracommissural nucleus of the ventral telencephalon (Vs-l) has low density scattered fibers (Figure 5e, f).

### Diencephalon and mesencephalon

Overall, NPY-ir cells and fibers exist in great quantity throughout the diencephalon and mesencephalon of *A. burtoni* (Figure 5). NPY-ir cells lie in the entopeduncular nucleus (E) (Figures 5e, f, 6d), the parvocellular preoptic nucleus, anterior part (nPPa) (Figures 5e, 6e), parvocellular preoptic nucleus, posterior part (nPPp), magnocellular preoptic nucleus parvocellular division (nPMp) (Figure 5e, f), dorsal (NLTd), medial (NLTm), and ventral (NLTv) parts of the lateral tuberal nucleus (Figures 5g, 6f), anterior tuberal nucleus (ATn) (Figures 5g, 6g), and paraventricular organ (PVO) (Figure 5g). Large cells (mean  $\pm$  SD diameter; Gravid:  $10.476 \pm 2.001 \mu\text{m}$ ; Brooding:  $10.867 \pm 1.471 \mu\text{m}$ ) with distinct ventrally projecting fibers are also found in the dorsal tegmental nucleus (DT) (Figures 5i, 6h). These cells are located in the same region as those identified as lying in the midbrain tegmentum of other fishes (Sakharkar et al., 2005; Subhedar, Cerda, & Wallace, 1996; Zahid, Malik, & Rani, 2014).

NPY-ir fibers lie in all preoptic nuclei including the nPPa, nPPp, magnocellular preoptic nucleus, parvocellular division (nPMp), magnocellular preoptic nucleus, gigantocellular division (nGMp), and nMMp (Figures 5d–f, 6e). Low density fibers are primarily present in the rostral nPPa with a moderately dense population of fibers just ventral to the anterior commissure (ac) (Figure 5d). Moderately dense to dense fibers are present in the area lateral to the rostral nPPa and ventral to the rostral E. Moderately dense fibers are also located in the nMMp, nPMp, nPPp, and nGMp (Figure 5f).

In the rostral hypothalamus, NPY-ir fibers lie in the NLTd, NLTm, NLTv, lateral tuberal nucleus intermediate part (NLTi), ATn, lateral part of the diffuse nucleus of the inferior lobe (NDILI), nucleus of the lateral recess (NRL), nucleus of the posterior recess (NRP), and posterior tuberal nucleus (NPT) (Figure 5g–k). Moderately dense varicose fibers are present in the ATn, which become denser towards the caudal ATn (Figure 5g). The rostral NLTd has fibers with large varicosities, and the NLTv, NLTi, and NLTm have moderately dense fibers. In more caudal regions of these nuclei, the fibers are less dense (Figure 5g). Low density fibers border the medial edge of the rostral NDILI, and in more caudal regions of NDILI, there are scattered, low density fibers positioned dorsally in

the region ventral to the tertiary gustatory nucleus (TGN) (Figure 5g–j). The rostral NRL has moderately dense fibers, while more caudal NRL regions have scattered fibers (Figure 5h–k). The caudal part of the diffuse nucleus of the inferior lobe (NDILc) has low density fibers in the medial area dorsal to the NRL (Figure 5j, k). Dense fibers are also present in the NRP (Figure 5h) and in the NPT.

The rostral portion of the dorsal posterior thalamic nucleus (DP) contains dense fibers throughout, while the density is lower in more caudal sections (Figure 5g). The central posterior thalamic nucleus (CP) has moderately dense fibers in rostral sections, but fibers are less dense and confined to the center of the nucleus in more caudal regions (Figure 5g). Moderately dense fibers are seen in the ventral habenular nucleus (nHv) and more scattered fibers in the dorsal habenular nucleus (nHd). Low to moderately dense fibers exist in most nuclei of this region, including PVO, periventricular nucleus of the posterior tuberculum (TPp), ventromedial thalamic nucleus (VMn), periventricular pretecal nuclei (PPv, PPD), anterior thalamic nucleus (An), nucleus pretecalis (NP), superficial pretecal nucleus intermediate division (PSi), lateral preglomerular nucleus (PGl), TGN, and nucleus of the torus lateralis (TLa), as well as regions adjacent to these nuclei (Figure 5g). Dense fibers are present in the central pretecal nucleus (NPC), central thalamic nucleus (CTn), and nucleus corticalis (NC). Fibers are primarily absent from the large PGn and corpus mammillare (CM) nuclei along the midline (Figure 5h, i), although there are an occasional few scattered varicose fibers in some sections.

Moderately dense NPY-ir fibers lie consistently in the tectum (T), primarily in the region between the periventricular gray zone (PGZ) and deep white zone of tectum (DWZ), but were also scattered throughout the central zone (CZ) and superficial gray and white zone (SWGZ) (Figure 5f–k). Low density fibers are found in the lateral tegmental nucleus (LT), DT, nucleus of the medial longitudinal fasciculus (nMLF), oculomotor nucleus (Illn), and glomerular nucleus (Gn) (Figure 5h–j). Low to moderately dense fibers are also found in the torus semicircularis (TS), specifically the central nucleus of TS (TSc), with scattered fibers in the ventrolateral nucleus (TSvl) (Figure 5h–k). Moderately dense fibers lie in the central part of the nucleus of the lateral valvulae (NLVc) and paratoral tegmental nucleus (PTT) (Figure 5i–j).

### Rhombencephalon

NPY-ir cells lie in the central gray (CG) surrounding the fourth ventricle (Figure 5k), and in the inferior olive (Figure 5m). In general, NPY-ir fibers are scarcer in the rhombencephalon compared to the telencephalon, diencephalon and mesencephalon. Scattered fibers are present in the Purkinje cell layer of the corpus cerebelli (CCeP) and valvula cerebelli (VCeP) (Figure 5k, l). Low to moderately dense fibers exist in the secondary gustatory nucleus (SGn), and the region lateral to the isthmal nucleus (NI) (Figure 5k). Low density fibers are found throughout the rostro-caudal CG (Figure 5j, k), as well as scattered fibers in NI, medial longitudinal fasciculus (mlf) (Figure 5j–l), Raphe nucleus (SR), interpeduncular nucleus (IP), and within several octavolateralis nuclei (Figure 5k, l). Dense fibers lie in the region between the medial reticular nucleus and secondary gustatory tract (sgt) (Figure 5l). Low density fibers are also present in the inferior (Ri), medial (Rm), and superior (Rs)



nuclei of the reticular formation (Figure 5j, l). Moderately dense to dense fibers are found bordering the dorsal portion of the vagal lobe (VL) and moderately dense fibers are present within the VL (Figure 5m). Low to moderately dense fibers lie in the medial funicular nucleus (MFN) and descending trigeminal tract (dtt) (Figure 5n).

### 3.2.1 | Localization of *npv* neurons - ISH

In the olfactory bulbs, *npv* cells are abundant in the ICL, which was not observed with antibody staining (Figure 7a). In the telencephalon, some scattered cells are found along the midline in Dm-1 and in the rostral DI-d and Dc, while cells are numerous in the subpallial Vv, dorsal part of the ventral telencephalon (Vd), Vc, VI, Vi, Vp, and supracommissural nucleus of the ventral telencephalon (Vs) (Figure 7b,c). Cells within some of these ventral telencephalic regions (notably the Vs), however, did not appear stained with IHC. *npv* cells are also found in the entopeduncular nucleus, nPPa, nPPp, and nMMp, and in the region ventral to the habenula (possibly in the nucleus of the thalamic eminentia, nTE) (Figure 7d). Similar to IHC, cells are also expressed in the ATn, PVO, and NLT (Figure 7e). In the mesencephalon, *npv* cells are abundant in the PGZ of the tectum (Figure 7e), and some scattered cells in the torus semicircularis (primarily TSc). No cells were observed in any cerebellar nuclei (valvula or corpus cerebelli). In the rhombencephalon, cells lie in the SGn and secondary visceral nucleus (SVn), and scattered cells are found in the CG below the fourth ventricle, in the inferior olive nucleus (IO), in reticular formation nuclei, and in the MFN of the rostral spinal cord above the central canal (Figure 7f, h). Overall, there are many more cells stained with ISH compared to IHC, including some that were not labeled at all with IHC (e.g., PGZ, IO, SGn, SVn, Vs, ICL, etc.) and some that stained intensely with IHC but were only weakly stained with ISH (e.g., gTN, DT).

### 3.2.2 | Localization of AGRP-immunoreactivity

#### Olfactory bulbs and telencephalon

There are no AGRP-ir cells in the olfactory bulbs. A few scattered -ir fibers lie in the ventro-medial area of the ECL and in the medial area of the ICL (Figure 8a).

There are also no AGRP-ir cells found anywhere in the telencephalon, but AGRP-ir fibers lie in both dorsal and ventral telencephalon regions (Figure 8a-d). In the dorsal telencephalon, low density scattered fibers are present in the rostral portion of Dm-1, Dc-1, DI-d, and DI-v2 (Figure 8a-c). Fibers are primarily absent from the medial part of the dorsal telencephalon (Dm), with the exception of scattered fibers in rostral Dm-1 (Figure 8a). In the ventral telencephalon, moderately dense AGRP-ir fibers lie in the rostral Vs-m, and scattered moderately dense fibers in the Vd-r and the caudal subdivision of Vd (Vd-c) (Figure 8b, c). Dense to moderately dense fibers are found throughout Vv (Figure 9a), as well as scattered fibers in the region lateral to the caudal portion of Vv and within Vp (Figure 8b, d).

#### Diencephalon and mesencephalon

AGRP-ir cells lie in the NLT; the rostral portion of the NLTv contains cells along the lateral edge that are then located in a more medial position in the caudal portion of this nucleus (Figures 8f, 9d).

In the preoptic nuclei, AGRP-ir fibers are abundant in the nPPa, nMMp, nPMp, nPPp, and nGMp (Figures 8d, e, 9b). Dense fibers are present in the nPPa and nPMp, while moderately dense fibers are present in the nPPp (Figure 8d, e). The rostral nMMp contains moderately dense fibers, which increase in density towards the caudal nMMp (Figure 8d). The regions lateral to these preoptic nuclei also contains moderately dense fibers (Figure 8d).

In the hypothalamus, low density AGRP-ir fibers lie in NLTd, NLTi, NLTm, and NLTv (Figures 8e, f, 9c, d). Low to moderately dense fibers also lie in ATn (Figures 8f, 9f), and scattered fibers are present in some more caudal diencephalic regions such as the medial nucleus of the interior lobe (NMIL) bordering the ventral side of the glomerular nucleus (Gn), and in NDILI (Figure 8g, h). Fibers are scattered in the NRL and are present throughout the entire rostro-caudal extent of this nucleus (Figures 8g-j, 9e).

In the thalamic region, scattered fibers exist in DP, CP, and VMn, as well as in ventral (nHv) and dorsal (nHd) nuclei of the habenula (Figure 8e, f). Scattered, low density fibers are also present in the posterior tuberal nucleus (PTN) and TPp (Figure 8f). The tectum consistently contains scattered AGRP-ir fibers located in the CZ, PGZ, DWZ, and SWGZ (Figure 8e, h). Scattered, low density fibers are present in the medial portion of Illn (Figure 8h). Scattered fibers also exist in the rostral PTT, the torus semicircularis (TSc and TSvl), and in regions surrounding Gn and the medial preglomerular nucleus (PGm) (Figure 8g, h).

#### Rhombencephalon

No AGRP-ir fibers are seen in the corpus or valvula cerebelli. Scattered low density AGRP-ir fibers lie in the rostral CG around the fourth ventricle. In more caudal regions of CG, there is an increase in fiber density (Figure 8j), but it is again low in the most caudal portion of the CG (Figure 8k). Moderately dense fibers are present in the area between the CG and Rs, and scattered fibers lie within reticular nuclei (Rs, Rm, Ri) (Figure 8j-l), SGn, SR, facial lobe, vagal lobe (VL), and the MFN of the rostral spinal cord (Figure 8j-m).

### 3.2.3 | Localization of *agrp* neurons - ISH

ISH labels *agrp* neurons solely within the hypothalamic NLTv, which is consistent with the somata labeling observed with IHC (Figure 2a, b).

### 3.2.4 | Localization of CART-immunoreactivity

#### Olfactory bulbs and telencephalon

There are no CART-ir cells in the olfactory bulbs. CART-ir fibers lie primarily in the ICL, but there are also some scattered fibers in the ECL and lateral margin of the rostral GL (Figure 8a).

In the telencephalon, CART-ir cells lie in the rostral Vv (Figures 8b, c, 10c), in VI (Figure 8b), and in the lateral part of Vc (Figures 8b, c, 10a). CART-ir fibers are found to some extent in all parts of the dorsal telencephalic nuclei (Figure 8a-d). Low density CART-ir fibers lie in DI-v1, DI-v2, and dorsal portion of DI-d (Figure 8a-c), while scattered fibers are present in all Dm regions (Figure 8a-d), throughout Dd, and in the posterior part of the dorsal telencephalon (Dp) (Figure 8d). CART-ir fibers also lie in all Dc regions, with moderate fiber densities in some rostral regions of Dc-1 and the lateral region of Dc-2, and more



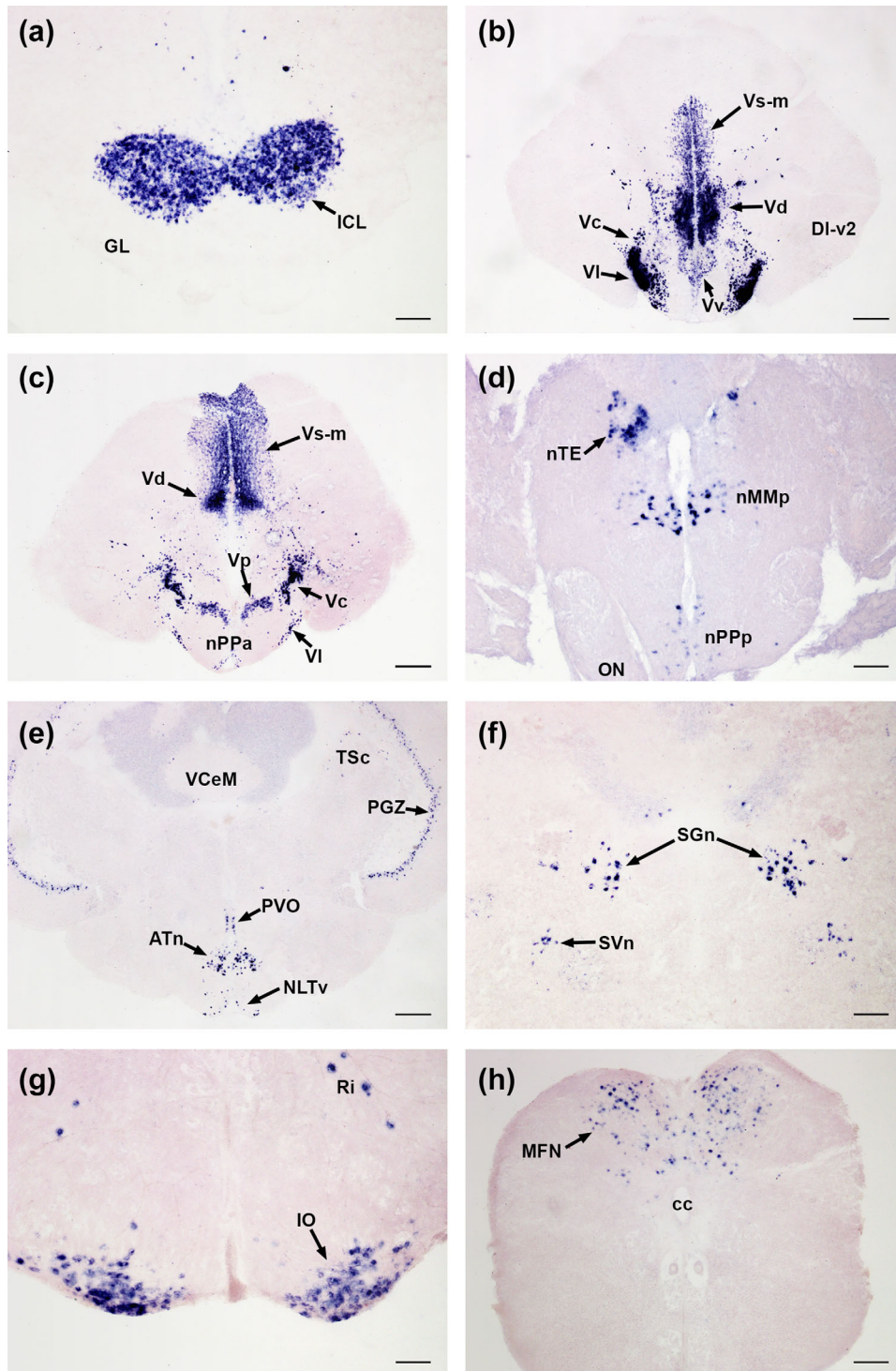


**FIGURE 7** Representative photomicrographs of *npy*-expressing cells in the brain of *A. burtoni*. Cells are abundant in the ICL of the olfactory bulb (a), and in subpallial nuclei of the ventral telencephalon, including Vv, VI, Vc, Vd, Vs-m, and Vp (b, c). *npy* cells also lie in pre-optic nuclei nPPa, nPPp, and nMMp, as well as nTE (c, d). Cells lie in the PVO, ATn, and NLTV regions, as well as the PGZ of the tectum, and TSc (e). In the rhombencephalon, *npy*-expressing cells are found in the SGn, SVn, IO, Ri, and MFN of the rostral spinal cord (f, h). Scale bars = 100  $\mu$ m (a, d, f, h), 250  $\mu$ m (b, c, e), 50  $\mu$ m (g). [Color figure can be viewed at [wileyonlinelibrary.com](http://wileyonlinelibrary.com)]

scattered distributions in caudal Dc-1, and in Dc-3, Dc-4 and Dc-5 (Figure 8a-d).

CART-ir fibers are also present to some extent in all parts of the ventral telencephalic nuclei (Figure 8b-d). Fibers exist in low density in the rostral

Vd-r, with a transition to moderate density in more caudal regions (Figure 8b, c). Low density scattered fibers are also present in Vv, VI, Vc, and Vp (Figure 8b-d). In the Vs-m, low density fibers are found in rostral sections bordering the dorsal portion of Vd-c, and then become scattered throughout

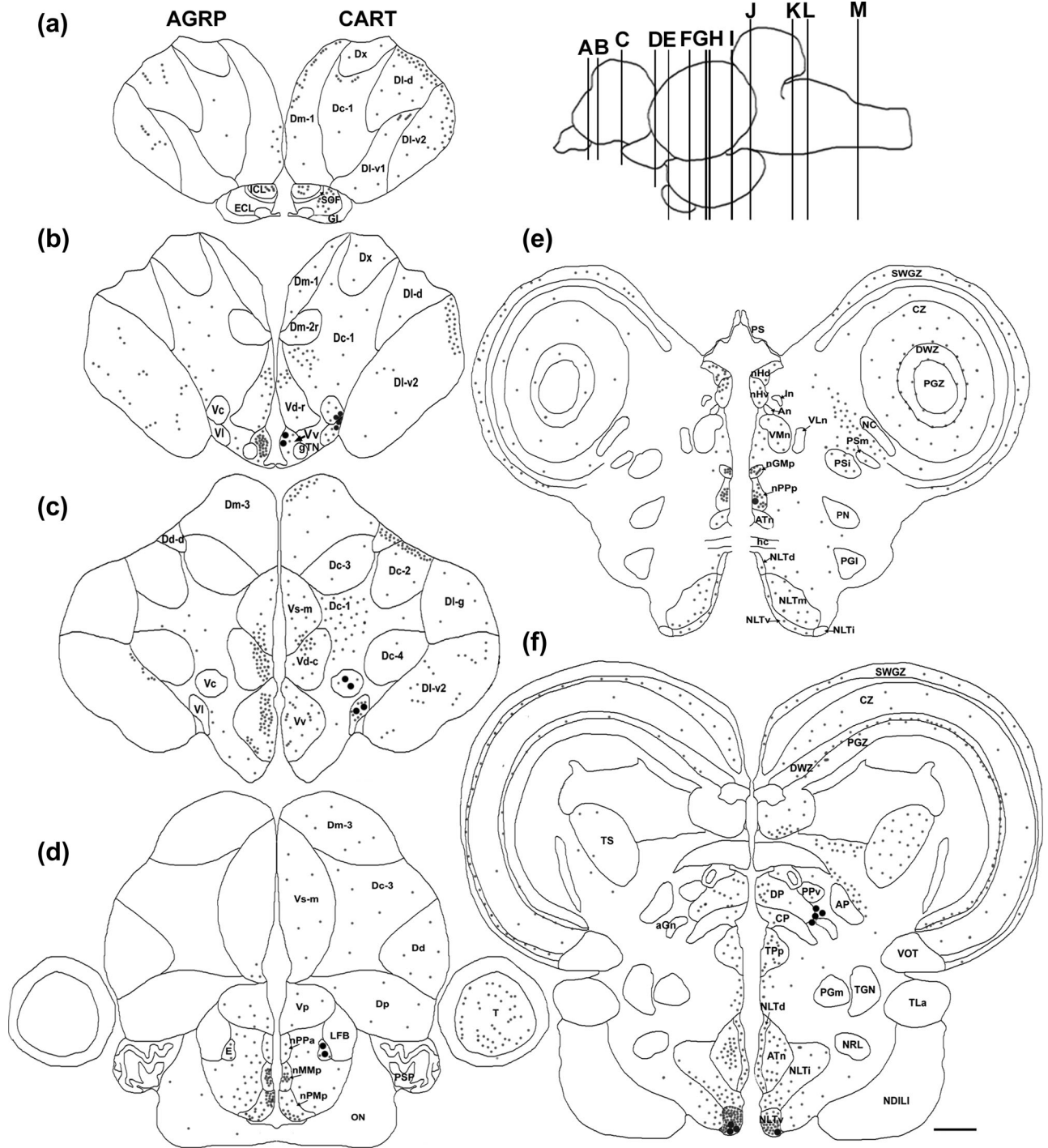


**FIGURE 8** Localization of AGRP (left half)- and CART (right half)-immunoreactivity in the brain of *A. burtoni*. Representative line drawings of transverse sections from rostral (a) to caudal (m) brain regions show the locations of AGRP and CART ir-somata (large black dots) and fibers (small black dots). Left side of brain shows AGRP distribution and right side shows CART distribution, along with labels of nuclei and other neuroanatomical structures. Figure inset at the top right shows a lateral view of the brain indicating the approximate levels of the corresponding transverse sections. Scale bar = 250  $\mu$ m. See list for abbreviations

the caudal extent of Vs-m (Figure 8c, d). In the Vd-c, low density fibers lie in the dorsal region bordering the ventral portion of Vs-m (Figure 8c).

**Diencephalon and mesencephalon**

CART-ir cells lie in the entopeduncular nucleus (E) (Figures 8d, 10b), medial area of the ventral nPPp (Figures 8e, 10d), NLTv

(Figures 8f, 10e), and NRP (Figures 8g, 10g). A small group of CART-ir cells also lies in the thalamus just lateral to DP and CP (Figures 8f, 10f). Large CART-ir cells (mean  $\pm$  SD diameter: Gravid:  $9.543 \pm 1.146 \mu$ m; Brooding:  $9.663 \pm 1.180 \mu$ m) are also found in the medial region of the nMLF situated dorsal to the mlf, and in DT (Figures 8g, h, 10h).

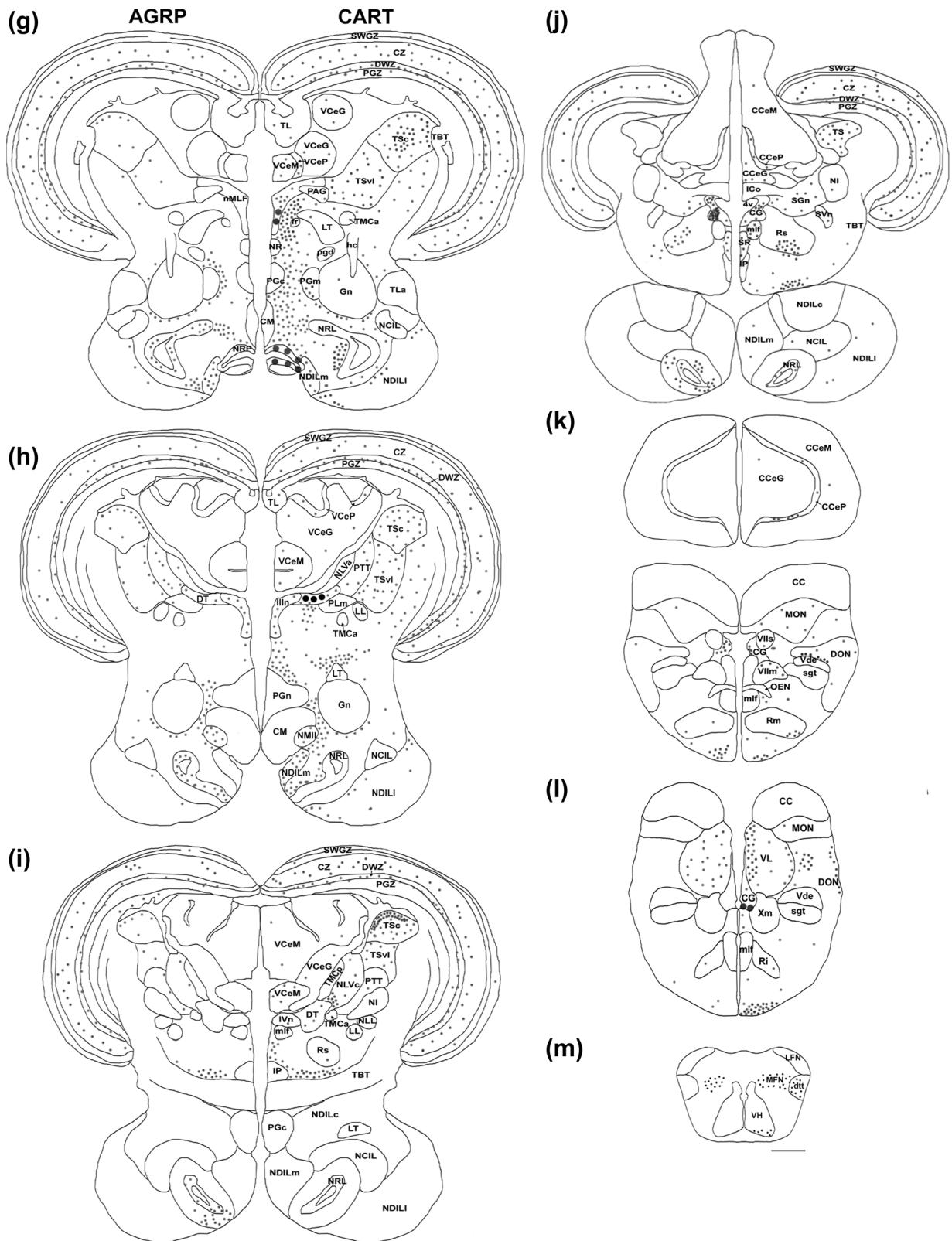
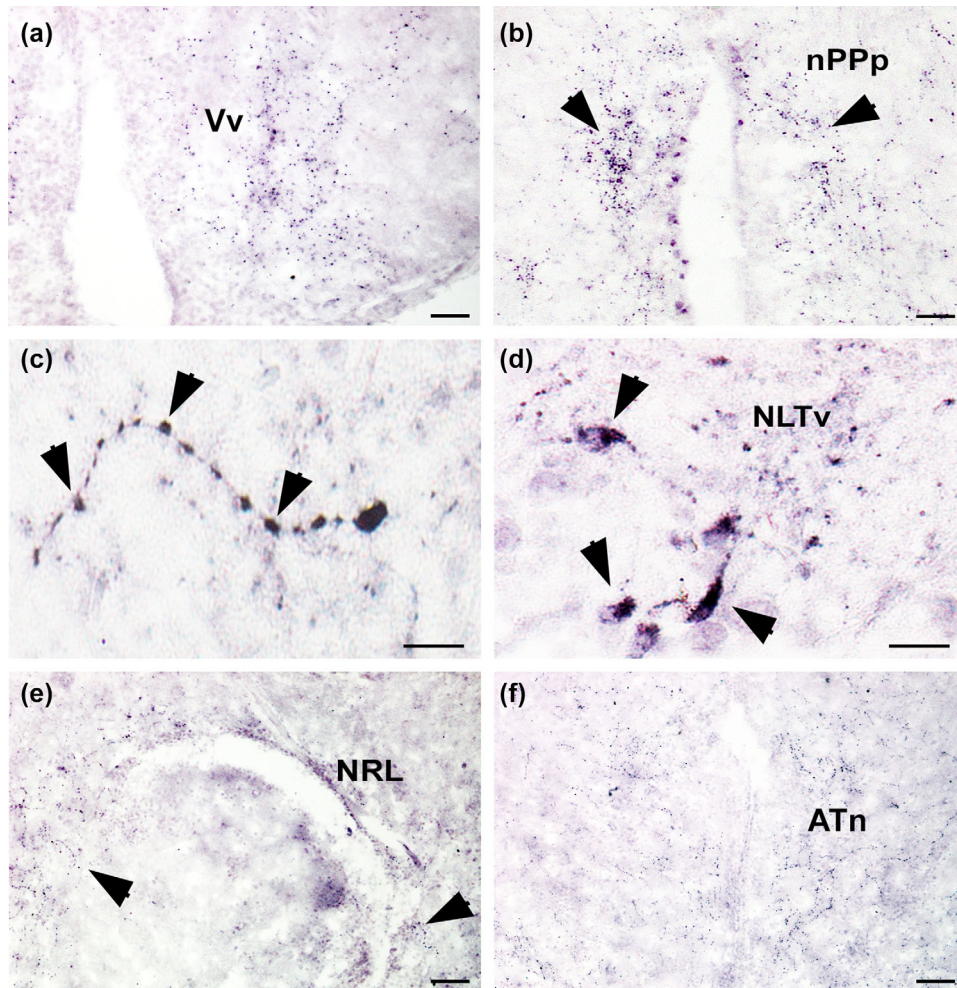


FIGURE 8 (Continued)

Moderately dense CART-ir fibers are present in the preoptic nuclei of the diencephalon, including nPPa, nPMp, nMMp, nGMP, and nPPp (Figure 8d, e). In the hypothalamus, fibers are present in NLTv, NLTd, NLTi, NDILI, NRL, and medial part of the diffuse nucleus of the inferior

lobe (NDILm) (Figure 8f, i). The NLTv, NLTi and ATn have low to moderately dense fibers scattered throughout their rostro-caudal extents, while the rostral NLTd has only a few scattered fibers (Figure 8f). The NRL has low to moderately dense fibers located around the lateral





**FIGURE 9** Representative photomicrographs of AGRP-immunoreactive somata and fibers in the brain of *A. burtoni*. Coronal sections of the diencephalon show immunoreactive fibers in Vv (a). Moderately dense fibers (arrowheads) in nPPp (b). Immunoreactive fibers with large varicosities (arrowheads) in NLTv of the hypothalamus (c). AGRP-ir cells (arrowheads) and fibers in NLTv (d). Scattered fibers (arrowheads) are present in the NRL surrounding the lateral recess (e), and in the ATn (f). Scale bars = 25  $\mu\text{m}$  in (a, b, e); 10  $\mu\text{m}$  in (c, d); 50  $\mu\text{m}$  in (f). See list for abbreviations. [Color figure can be viewed at [wileyonlinelibrary.com](http://wileyonlinelibrary.com)]

recess with fibers primarily on the medial side in the region just dorsal to the NDILm (Figure 8i). The NDILI has a few scattered fibers throughout the nucleus while more dense fibers are found dorsally between the NDILI and the Gn and NMIL (Figure 8i).

CART-ir fibers are found to some extent throughout all thalamic and pretectal nuclei (Figure 8e, f). In the thalamus, DP, CP, and VMn contain scattered low density CART-ir fibers (Figure 8e, f). The PPD and PPv have scattered low density fibers confined to the dorsal portion of the nucleus that borders the posterior commissure (pc). The nTE has low density fibers confined to the medial portion of the nucleus. The TPp has a few scattered fibers throughout its rostro-caudal extent (Figure 8f), and low density fibers are found bordering the ventral area around the Gn (Figure 8h).

In the tectum, fibers lie consistently throughout the SWGZ, DWZ, CZ, and PGZ (Figure 8d–k). The SWGZ has scattered fibers while there are more numerous fibers in CZ, and dense fibers between the DWZ and PGZ (Figure 8e–k). CART-ir fibers are dense along the midline in the mesencephalon, with regions such as PGn, CM, and Gn either

devoid of fibers or containing only a few scattered fibers (Figure 8g, h). The regions surrounding these nuclei, however, contain moderate to high density fibers. The Illn, nMLF, LT, and DT contain some scattered fibers (Figure 8h–i). The torus longitudinalis (TL) also has a few scattered fibers throughout its rostro-caudal extent (Figure 8g, h). CART-ir fibers are abundant in the TS, with moderate to dense fibers in TSc, particularly along the dorsal margin, and moderate to low density fibers in TSvl (Figure 8g–j). The PTT and NLVc also contain scattered CART-ir fibers (Figure 8h–i).

#### Rhombencephalon

Overall, CART-ir fibers are scattered and less numerous in the rhombencephalon compared to more rostral brain areas (Figure 8j–m). Some scattered fibers lie in the granular (VCeG) and molecular (VCeM) layers of valvula cerebelli, with slightly greater densities found in VCeP (Figure 8g–i). Similarly, low density fibers lie in CCeP, with some occasional scattered fibers in the granular (CCeG) and molecular (CCeM) layers of corpus cerebelli (Figure 8j, k). CART-ir fibers are scattered in SGN, but

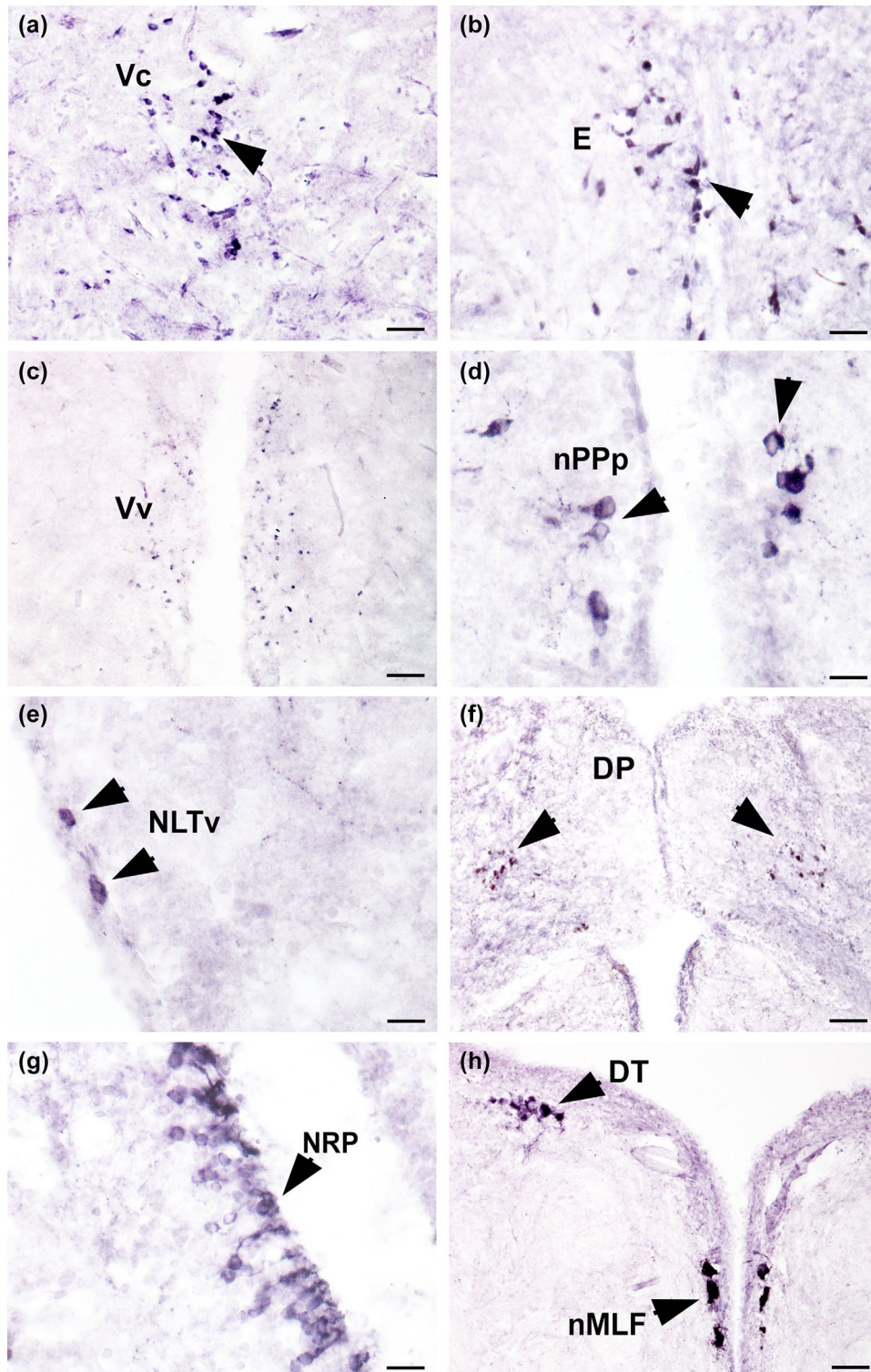


**FIGURE 10** Representative photomicrographs of CART-immunoreactive somata and fibers in the brain of *A. burtoni*. Coronal sections of the telencephalon show CART-ir cells (arrowheads) in the Vc (a) and entopeduncular nucleus (b). Small CART-ir cells in Vv (c). Immunoreactive cells (arrowheads) in the nPPp (d) and NLTv (e). A group of small CART-ir cells lies in the thalamus adjacent to DP (f). CART-ir cells in NRP (g). Large immunoreactive cells are also present in DT and along the midline in nMLF (h) of the mesencephalon. Scale bars = 25  $\mu$ m in (a, b, d); 50  $\mu$ m in (c, f, h); 10  $\mu$ m in (g, e). See list for abbreviations. [Color figure can be viewed at [wileyonlinelibrary.com](http://wileyonlinelibrary.com)]

only an occasional sparse fiber is seen in NI (Figure 8j). The rostral CG has a few scattered fibers bordering the fourth ventricle and moderately dense to dense fibers in the caudal CG (Figure 8k, l). Rs and Rm

have low density scattered fibers throughout, and a few fibers are seen within the mlf (Figure 8j–l). Low density CART-ir fibers are scattered in SR along the midline (Figure 8j), in all octavolateralis nuclei of the



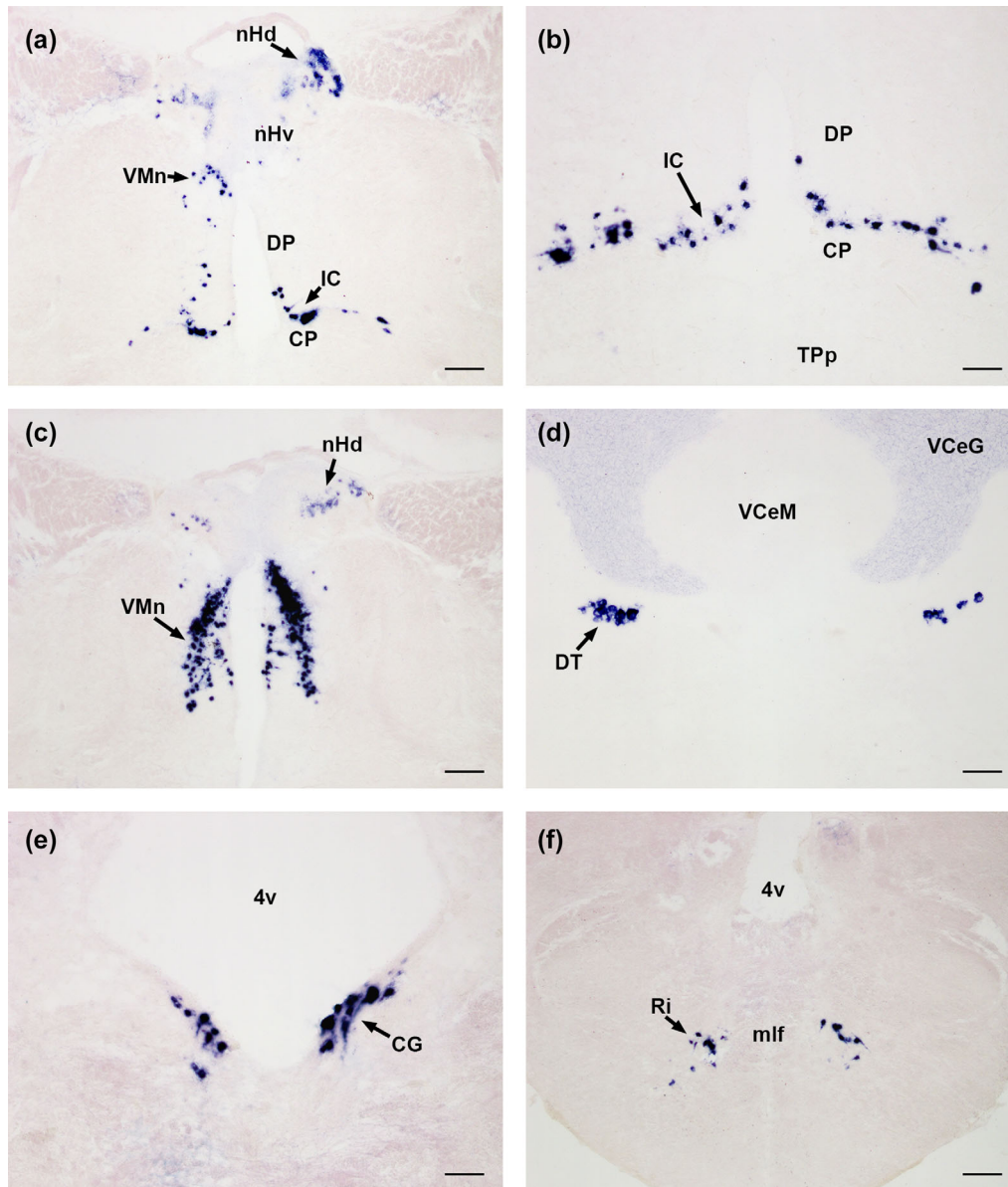


**FIGURE 11** Representative photomicrographs of *cart4*-expressing cells in the brain of *A. burtoni*. *cart4* cells in the habenula (nHd), and thalamic VMn and IC (a–c). Cluster of large cells in DT (d). In the hindbrain, *cart4* cells are found in the CG and Ri (e–f). Scale bars = 100  $\mu\text{m}$  (a, c, d, f), 50  $\mu\text{m}$  (b, e). [Color figure can be viewed at [wileyonlinelibrary.com](http://wileyonlinelibrary.com)]

hindbrain, in the facial lobe, and along the ventro-lateral regions of the hindbrain (Figure 8j–l). Low density fibers are also found throughout the VL (Figure 8l), while low to moderately dense fibers lie in the MFN and dtt of the rostral spinal cord (Figure 8m).

### 3.2.5 | Localization of *cart2* and *cart4* – ISH

The distribution of *cart4* cells in the brain is more restricted than the widespread staining of *cart2* neurons (Figure 11). No *cart4* cells are detected in the telencephalon, and notably, *cart4* cells are absent from NLT. *cart4* cells lie in the habenula (nHd), VMn, intercalated nucleus (IC), and TPP (Figure 11a–c). A distinct cluster of large *cart4* cells lies in DT (Figure 11d), and in the rhombencephalon, cells are found in CG, Ri, and scattered within the sensory VL

(Figure 11e, f). The only *cart4* cells labeled with the CART antibody are those in DT.

In contrast to *cart4*, *cart2* cells are abundant and widely distributed throughout the entire brain (Figure 12). Numerous cells lie in the ICL of the olfactory bulbs (Figure 12a), and some scattered cells are seen in rostral Dm, Dd, and lateral parts of the dorsal telencephalon (DI). Numerous *cart2* cells also lie within several Dc nuclei (Dc-3, -4, -5), along with more sparse cells in Dc-1 (Figure 12b–d). *cart2* cells are abundant in Vv, Vc, VI, and Vi of the subpallium (Figure 12b, c). In the preoptic nuclei, *cart2* cells localize primarily to nPPa, nPPP, and nMMp (Figure 12c, e). Moving caudally, *cart2* cells lie in many diencephalic and mesencephalic regions including the parvocellular superficial pre-tectal nucleus (PSP), PPd, PPv, prethalamus (PN), PGm, PGI, DP,

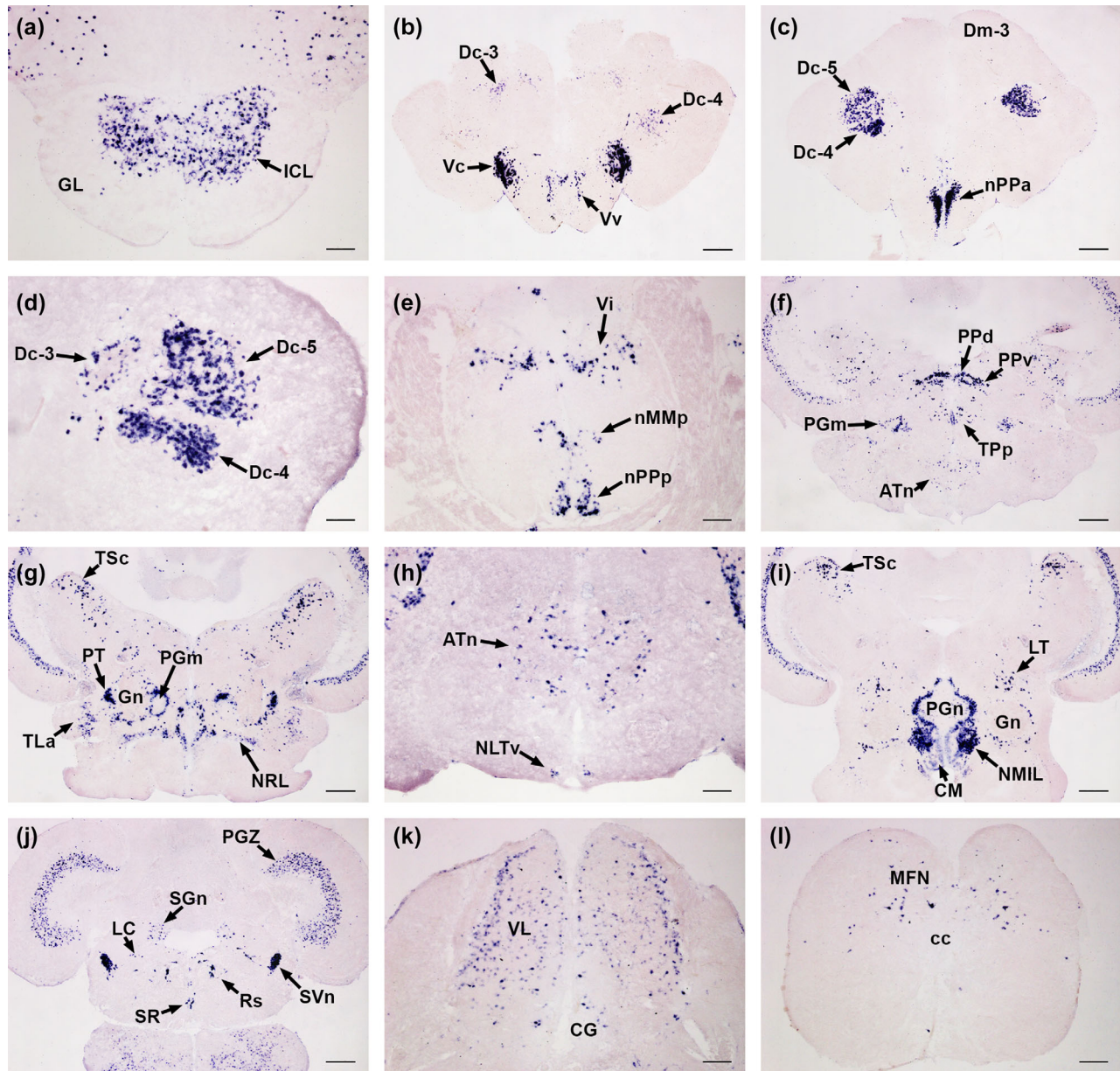


**FIGURE 12** Representative photomicrographs of *cart2*-expressing cells in the brain of *A. burtoni*. *cart2*-expressing cells are abundant in the ICL of the olfactory bulb (a). In the telencephalon, numerous *cart2* cells lie in subpallial Vc/VI, Vv, and Vi regions, as well as pallial Dc-3, -4, and -5 (b–e). *cart2* cells are expressed in preoptic nuclei nPPa, nPPp, and nMMp (c, e). *cart2* cells in the PPd, PPv, TPa, ATn, and PGm (f). Cells lie in several diencephalic and mesencephalic regions, including PT, TLa, TSc, and NRL, and cells surround some nuclei such as PGm (g). The ATn and NLTv have *cart2*-expressing cells (h). Cells lie in TSc, LT, CM, and NMIL, and cells surround Gn and PGn (i). *cart2* cells also lie in the PGZ of the tectum, SGn, SVn, LC, SR, and Rs (j). In the rhombencephalon, *cart2*-expressing cells are found in the sensory vagal lobe (VL) and MFN of the rostral spinal cord (k, l). Scale bars = 100  $\mu\text{m}$  (a, d, e, h, k, l), 250  $\mu\text{m}$  (b, c, f, g, i, j). [Color figure can be viewed at [wileyonlinelibrary.com](http://wileyonlinelibrary.com)]

TPp, PVO, ATn, NLT, posterior thalamic nucleus (PT), TLa, nMLF, NPT, NRP, CM, NMIL, and NRL (Figure 12f–i). Cells also surround PGn and Gn, and are present in LT, TS (primarily TSc), and PGZ of the tectum (Figure 12g, i, j). In the rhombencephalon, distinct *cart2* cells lie in CG, SGn, SVn, LC, SR, IO, and reticular formation nuclei (Figure 12j). *cart2* cells are also scattered in the sensory VL, throughout most hindbrain octavolateralis nuclei, and in the MFN of the rostral spinal cord (Figure 12k, l). No cells exist in any cerebellar nuclei (valvula or corpus

cerebelli). The *cart2* neurons that are also labeled with CART IHC include Dm-1, Vc/VI, nPPp, nMLF, and NRP.

### 3.3 | Reproductive state differences in somata size

NPY-ir (mean  $\pm$  SE; Gravid:  $19.792 \pm 0.869 \mu\text{m}^2$ ; mouth brooding:  $13.057 \pm 0.918 \mu\text{m}^2$ ) and AGRP-ir (Gravid:  $16.035 \pm 0.636 \mu\text{m}^2$ ; mouth brooding:  $11.672 \pm 0.636 \mu\text{m}^2$ ) mean somata sizes in the NLT are



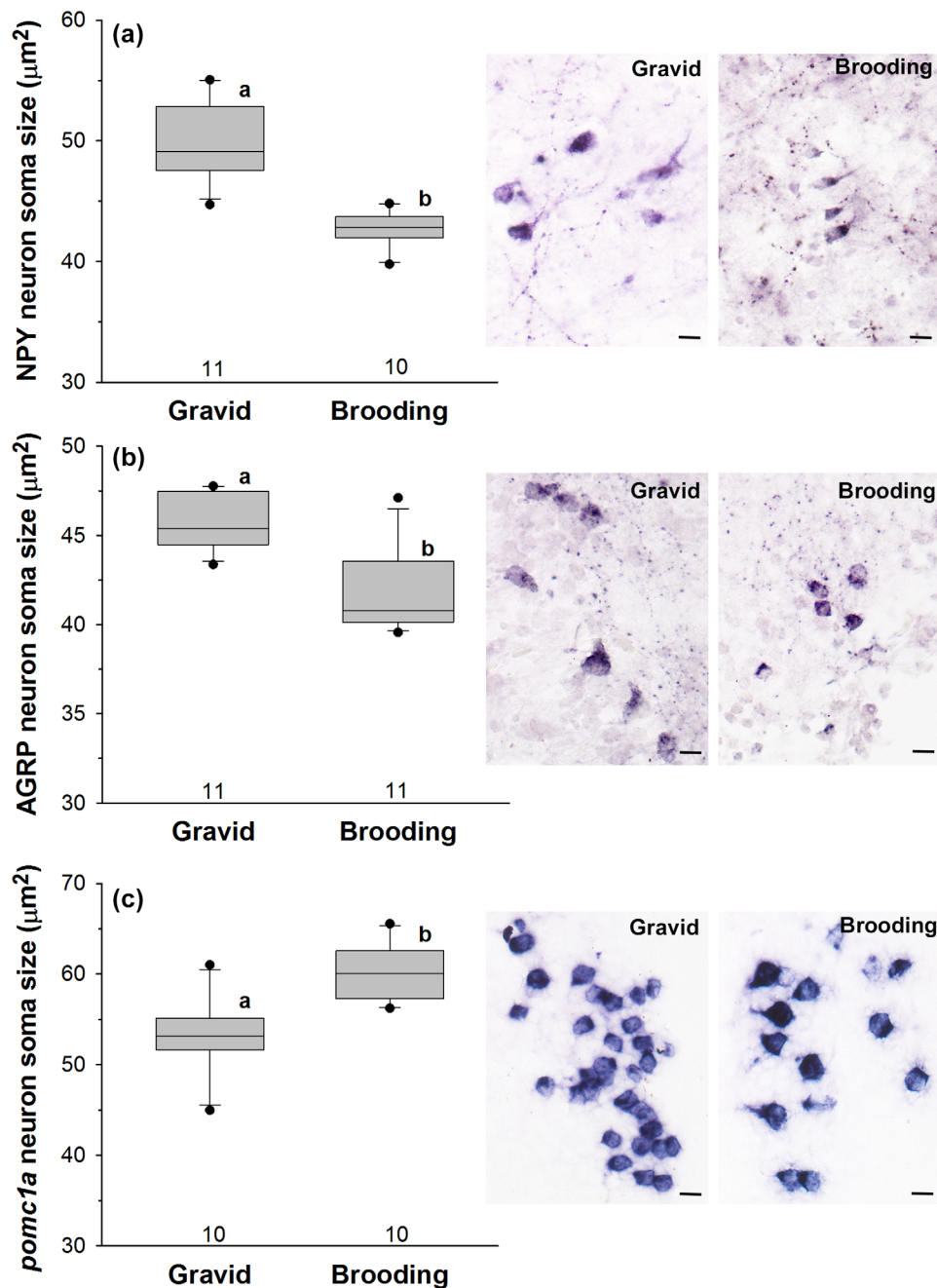


**FIGURE 13** Reproductive state differences in somata sizes of AGRP, NPY, and *pomc1a* neurons in the lateral tuberal nucleus of *A. burtoni* females. NPY-ir (a) and AGRP-ir (b) somata sizes are larger in gravid compared to brooding females, while *pomc1a* (c) neurons are larger in brooding compared to gravid females. In each graph, the bottom of each box is the 25th percentile, the top is the 75th percentile and the line in the middle is the median. Whiskers (error bars) indicate the 10th and 90th percentiles and dots represent points outside the 10th–90th percentile. Sample sizes (number of fish analyzed) are indicated beneath each plot. Different letters indicate statistical differences at  $p < 0.05$ . Representative stained transverse sections through the NLT for gravid and brooding females are shown at right. Scale bars = 10  $\mu\text{m}$ . [Color figure can be viewed at [wileyonlinelibrary.com](http://wileyonlinelibrary.com)]

larger in gravid females compared to brooding females (NPY: ANCOVA;  $F = 24.531$ ;  $df = 18$ ;  $p < 0.001$ ; AGRP: ANCOVA;  $F = 20.529$ ;  $df = 19$ ;  $p < 0.001$ ) (Figure 13a, b). *Pomc1a* mean somata sizes are larger in brooding compared to gravid females (ANCOVA;  $F = 19.401$ ;  $df = 17$ ;  $p < 0.001$ ) (Gravid:  $22.898 \pm 1.197 \mu\text{m}^2$ ; mouth brooding:  $30.702 \pm 1.197 \mu\text{m}^2$ ) in the NLT (Figure 13c). Correlations between somata sizes, GSI, and HSI for gravid and brooding females combined are summarized

in Table 3. There is a negative correlation between *pomc1a* somata size and GSI. *Pomc1a* somata size is also negatively correlated with both NPY-ir and AGRP-ir somata sizes. NPY-ir and AGRP-ir somata sizes both show a positive correlation with GSI. HSI is not correlated with any of the neuropeptide somata sizes. However, there were no significant correlations among any variables when gravid females (all  $r < 0.60$ ;  $p > 0.05$ ) and brooding females (all  $r < 0.40$ ;  $p > 0.05$ ) were run separately.



**TABLE 3** Correlations between somata sizes (NPY, AGRP, *pomc1a*), Gonadosomatic Index (GSI), and Hepatosomatic Index (HSI) for combined Gravid and Brooding *A. burtoni* females

	AGRP	<i>pomc1a</i>	GSI	HSI
NPY	0.653 0.001 <sup>a</sup>	-0.7821 <0.001 <sup>a</sup>	0.659 0.001 <sup>a</sup>	0.405 0.068
AGRP		-0.696 0.001 <sup>a</sup>	0.581 0.005 <sup>a</sup>	0.370 0.09
<i>pomc1a</i>			-0.480 0.032 <sup>a</sup>	-0.276 0.239

Correlation coefficients (*r*; top) and *p* values (bottom) are shown. Sample size was 20–22 fish for each comparison (10–11 individuals per reproductive state).

<sup>a</sup>Denotes significance at *p* < 0.05 from Pearson Correlation tests.

### 3.4 | Hypothalamic mRNA expression differences between gravid and brooding females

A total of 28 (15 gravid, 13 brooding) females were used in the hypothalamic mRNA analysis. Similar to the females used for neuropeptide-containing somata quantification analyses described above, gravid females have higher GSI (mean  $\pm$  SD;  $10.08 \pm 1.35$ ) (Mann–Whitney; *U* = 0.00; *p* < 0.001) and larger ova diameters ( $2.35 \pm 0.30$  mm) (Mann–Whitney; *U* = 0.00; *p* < 0.001) compared to brooding females ( $0.71 \pm 0.23$  mm). Gravid females also have higher HSI ( $1.66 \pm 0.61$ ) values compared to brooding females ( $0.86 \pm 0.33$ ) (Mann–Whitney; *U* = 19.00; *p* < 0.001), and higher condition factors compared to brooding females (gravid:  $3.90 \pm 0.41$ ; mouth brooding:  $3.06 \pm 0.43$ ) (Student's *t* test; *p* < 0.001; *t* = 5.346; *df* = 26), indicative of greater energy reserves and overall fitness. Standard length (Student's *t* test; *p* = .152; *t* = -1.475; *df* = 26) and body mass (Student's *t* test; *p* = 0.0796; *t* = 1.824; *df* = 26) did not differ between gravid and brooding females. Macro-dissected hypothalamic mRNA levels for *agrp*, *cart2*, *cart4*, *ghrelin receptor (ghs-r1)*, *leptin receptor (lepr)*, *npv*, and *pomc1a* were compared between gravid and brooding females. *Agrip* mRNA expression is significantly higher in gravid females compared to brooding females, but there are no differences between gravid and brooding females for any of the other mRNA levels measured (Table 4). Correlations between hypothalamic mRNA levels for all fish combined are

summarized in Table 5. *Pomc1a* mRNA levels positively correlate with *agrp* mRNA levels in the hypothalamus, and *npv* mRNA levels positively correlate with mRNA levels of the receptors, *ghs-r1* and *lepr*. When gravid and brooding animals were analyzed separately, only a single positive correlation between *lepr* and *agrp* was evident in brooding females (*r* = 0.75, *p* = 0.021). In contrast, gravid females showed many positive correlations between candidate gene mRNA levels in the hypothalamus: *pomc1a* with *agrp* (*r* = 0.74, *p* = 0.003), *cart2* (*r* = 0.55, *p* = 0.04), and *npv* (*r* = 0.68; *p* = 0.007); *agrp* with *ghs-r1* (*r* = 0.61, *p* = 0.02), *cart2* (*r* = 0.75, *p* = 0.002), *lepr* (*r* = 0.61, *p* = 0.015), and *npv* (*r* = 0.80, *p* < 0.001); *ghs-r1* with *lepr* (*r* = 0.59, *p* = 0.03); *cart2* with *lepr* (*r* = 0.72, *p* = 0.003) and *npv* (*r* = 0.83, *p* < 0.001); and *lepr* with *npv* (*r* = 0.85, *p* < 0.001).

## 4 | DISCUSSION

Our results provide the first localization maps of NPY, AGRP, and CART neurons throughout the entire brain of a mouth brooding teleost fish. We demonstrate that these neuropeptides are found in brain regions that regulate feeding, energy status, and reproduction that are conserved with those of higher vertebrates. Future studies should conduct co-labeling experiments to test whether any of these neuropeptides are expressed in the same or different neurons, particularly in the NLT. Further, we show that somata size of *pomc1a*, AGRP, and NPY-producing neurons differs between gravid and mouth brooding *A. burtoni* females, suggesting that changes in the synthesis, release, or neural activity of these neurons is important for regulating cyclical variations between these different energetic and reproductive states.

### 4.1 | Comparisons of NPY, AGRP, and CART with other teleosts Neuropeptide Y (NPY)

Moderate NPY-immunoreactive fibers were detected in all layers of the olfactory bulb (ECL, ICL, GL, SOF) in *A. burtoni*, which is similar to other fish species including tilapia (Sakharkar et al., 2005), goldfish (Pontet et al., 1989), and the ayu (Chiba, Oka, & Honma, 1996). NPY-ir cells were not detected in the olfactory bulbs of *A. burtoni*, which is similar to the Senegalese Sole (Rodríguez-Gomez, Rendon-

**TABLE 4** Relative mRNA Levels in the Hypothalamus of Gravid and Mouthbrooding *A. burtoni* females

Gene	Gravid females	Mouthbrooding females	<i>F</i>	<i>df</i>	<i>p</i>
<i>agrp</i>	0.0146 $\pm$ 0.0153	0.00393 $\pm$ 0.00298	4.926	23	0.037*
<i>cart2</i>	1.15 $\times 10^{-8}$ $\pm$ 6.20 $\times 10^{-9}$	1.67 $\times 10^{-8}$ $\pm$ 1.14 $\times 10^{-8}$	2.284	25	0.143
<i>cart4</i>	4.0 $\times 10^{-10}$ $\pm$ 8.00 $\times 10^{-10}$	1.00 $\times 10^{-10}$ $\pm$ 2.00 $\times 10^{-10}$	1.851	24	0.186
<i>ghs-r1</i>	0.00226 $\pm$ 0.000953	0.00345 $\pm$ 0.00213	0.023	24	0.880
<i>lepr</i>	0.00226 $\pm$ 0.000953	0.00345 $\pm$ 0.00213	3.380	23	0.079
<i>npv</i>	1.99 $\times 10^{-8}$ $\pm$ 9.60 $\times 10^{-9}$	3.32 $\times 10^{-8}$ $\pm$ 2.79 $\times 10^{-8}$	3.099	25	0.091
<i>pomc1a</i>	0.00166 $\pm$ 0.000783	0.00172 $\pm$ 0.00132	0.001	25	0.974

Macro-dissected hypothalamic mRNA levels are normalized to the geometric mean of the reference genes *18s* and *rpl32* (see methods for details). Values are reported as mean  $\pm$  SD. Statistical values are results of ANCOVA, using hypothalamic mass as a covariate.

**TABLE 5** Correlations between hypothalamic mRNA Levels of candidate genes for combined gravid and mouth brooding *A. burtoni* females

	<i>agrp</i>	<i>ghs-r1</i>	<i>lepr</i>	<i>npy</i>	<i>cart2</i>	<i>cart4</i>
<i>pomc1a</i>	0.547 <b>0.004*</b>	0.220 0.281	0.316 0.124	0.233 0.243	-0.0967 0.631	-0.139 0.498
<i>agrp</i>		0.371 0.0678	0.362 0.0822	0.0215 0.917	-0.183 0.371	-0.0347 0.869
<i>ghs-r1</i>			0.281 0.164	0.506 <b>0.007*</b>	-0.370 0.0572	-0.265 0.191
<i>lepr</i>				0.501 <b>0.009*</b>	0.167 0.414	-0.0540 0.798
<i>npy</i>					-0.148 0.452	-0.137 0.495
<i>cart2</i>						0.188 0.348

Correlation coefficients (*r*; top) and *p* values (bottom) are shown. Sample size was 28 fish for each comparison (15 gravid, 13 brooding individuals).

\*Denotes significance at  $p < 0.05$  from Pearson Correlation tests.

Unceta, Sarasquete, & Munoz-Cueto, 2001), but differs from other species such as the goldfish (Pontet et al., 1989), senegal bichir (Reiner & Northcutt, 1992), and ayu (Chiba et al., 1996), in which NPY-ir cells were present in the ECL of the olfactory bulbs. However, *npy* mRNA was abundant in cells of the ICL in the olfactory bulbs in *A. burtoni*, which is consistent with that seen in the sea bass *Dicentrarchus labrax* (Cerde-Reverter et al., 2000). The presence of NPY-ir fibers and *npy* cells in the olfactory system suggests a modulatory role in olfactory processing, possibly related to appetite and hunger level of the animal, similar to that described in the axolotl (Mousley, Polese, Marks, & Eisthen, 2006).

In the telencephalon of *A. burtoni*, NPY-immunoreactive cells were found in the Vd-r, VI, Vc, and Dc, and -ir fibers were present throughout the dorsal and ventral telencephalon. This NPY-ir fiber pattern is generally similar to that reported in other teleosts (Batten, Cambre, Moons, & Vandesande, 1990; Chiba et al., 1996; Danger et al., 1991; Gaikwad et al., 2004; Kah et al., 1989; Pontet et al., 1989; Sakharkar et al., 2005; Subhedar et al., 1996). NPY-immunoreactivity in *A. burtoni* was also present in various regions that are homologous to mammalian nuclei involved in feeding and reproduction. For example, NPY-ir cells were present in the entopeduncular nucleus (E), which is consistent with findings in goldfish (Pickavance, Staines, & Fryer, 1992), rainbow trout (Danger et al., 1991), catfish (Gaikwad et al., 2004), killifish (Subhedar et al., 1996), and carp (Marchetti et al., 2000). While the definitive homolog of the entopeduncular region is not known in teleosts, the mammalian entopeduncular region is part of the amygdala (O'Connell & Hofmann, 2011). However, the entopeduncular nucleus is also thought to play a role in reproduction. In castrated male tilapia, for example, depletion of NPY immunoreactivity in E neurons was evident post-castration, but was restored following testosterone treatments (Sakharkar et al., 2005), suggesting a reproductive role for the NPY-ir cells in E. The prevalent NPY-immunoreactivity in the telencephalon of teleosts suggests widespread modulatory roles in reproduction, sensory processing, decision-making, and social and other life-history behaviors. For example, in the preoptic area of *A. burtoni*, NPY-ir cells were

present in nPPa, nMMp, and nPMp, and fibers were found throughout all preoptic nuclei. In teleosts, the importance of the preoptic area in reproduction is well established because it contains GnRH1 neurons that project directly to the pituitary to stimulate the synthesis and release of gonadotropin hormones. In *A. burtoni*, NPY-ir cells were also present in the NLT, the teleost homolog to the mammalian arcuate nucleus (Cerde-Reverter & Peter, 2003; Liu et al., 2010) involved in the control of energy balance and feeding behavior. Thus, the present study suggests that NPY's role in regulating feeding and reproductive functions is likely conserved.

## 4.2 | Agouti-Related Protein (AGRP)

AGRP-immunoreactivity in the olfactory bulb of *A. burtoni* was restricted to a few fibers in the ICL. This is similar to zebrafish where fibers were found in the olfactory bulbs, however, they were not restricted to a particular cell layer (Forlano & Cone, 2007). Therefore, the presence of AGRP in the olfactory bulbs of *A. burtoni* suggests a conserved neuroanatomical distribution, but examinations in more species are needed. The presence of AGRP in the olfactory bulb could suggest a role in olfactory processing, specifically in conjunction with the melanocortin system.  $\alpha$ -MSH-ir fibers are present in the olfactory bulbs of zebrafish and the MC4 receptor was present in the olfactory bulb of the spiny dogfish (Ringholm et al., 2003), suggesting that AGRP may modulate olfactory processing related to feeding and energetic status.

AGRP-ir cells in *A. burtoni* are found exclusively in the NLT of the hypothalamus. This is consistent with findings in goldfish (Cerde-Reverter & Peter, 2003), zebrafish (Forlano & Cone, 2007), and sea bass (Aguilleiro et al., 2014), where AGRP is mainly expressed in the caudal portion of the NLT. This region of the brain is associated with feeding and energy expenditure in teleosts (Forlano & Cone, 2007), and is considered the homolog of the arcuate nucleus in mammals because it expresses the specific arcuate markers, AGRP and POMC. In some fishes, fasting up-regulates brain mRNA levels of *agrp* [e.g., goldfish (Cerde-Reverter & Peter, 2003) and zebrafish (Song et al., 2003)],

while in other species fasting decreases *agrp* levels [e.g., common carp (Wan et al., 2012)]. Nevertheless, most studies suggest that AGRP also functions as a feeding modulator in teleost fishes. AGRP and NPY are co-expressed in the same neurons in mammals, but further double label studies are necessary to determine if this is also true in *A. burtoni* and other teleosts. Our study provides further evidence that the neuroanatomical distribution of AGRP is conserved and suggests that the mechanisms regulating energy homeostasis may be similar across vertebrates.

### 4.3 | Cocaine and amphetamine-regulated transcript (CART)

CART-immunoreactivity was absent from the SOF and gTN of *A. burtoni*, but CART-immunoreactive fibers were observed in the ICL, ECL, and GL of the olfactory bulb, which is consistent with previous findings in catfish (Singru et al., 2007) and zebrafish (Akash et al., 2014), suggesting a role for CART in the processing of olfactory information in teleosts. Similarly, in rats, low density CART-ir fibers were found in the inner plexiform layer, and CART-ir cells were present in the mitral and outer plexiform layers of the olfactory bulbs (Couceyro, Koylu, & Kuhar, 1997; Koylu, Couceyro, Lambert, & Kuhar, 1998). Further, CART peptide was found in the mitral cells of the rat olfactory bulb, suggesting a role for CART in the processing of olfactory signals in mammals as well (Couceyro et al., 1997; Koylu et al., 1998). In *A. burtoni*, *cart2* cells were also abundant in the ICL, which is consistent with that in the zebrafish (Akash et al., 2014). Taken together, these findings suggest a role for CART in the processing of olfactory information in vertebrates that warrants further investigation with a comparative approach. Further, the wide distribution of CART-ir fibers in brain regions that process other sensory information (e.g., visual, auditory, mechanosensory) in *A. burtoni* and other fishes (Mukherjee et al., 2012) suggests additional functions in sensory integration.

CART-immunoreactivity was also present in neuroendocrine regulatory areas of the telencephalon and diencephalon in *A. burtoni*. For example, CART-ir cells were present in the entopeduncular nucleus, which is congruent with studies done in the catfish (Mukherjee et al., 2012; Singru et al., 2007) and zebrafish (Akash et al., 2014). In contrast, however, CART-immunoreactivity was not observed in the entopeduncular nucleus of the frog *Rana esculenta* (Lazar, Calle, Roubos, & Kozicz, 2004). This suggests that there may be species or taxa-specific differences across vertebrates. CART-ir somata were also present in the nPPp of *A. burtoni*, and fibers were present throughout the preoptic nuclei, which is consistent with other teleosts. Further, *cart2* cells were detected in several preoptic nuclei via ISH in *A. burtoni*. In zebrafish, ISH experiments showed *cart2* and *cart4* cells in nPPa and nPPp (Akash et al., 2014), and immunostaining experiments demonstrated a dense CART-ir fiber network in the preoptic area (Mukherjee et al., 2012). In catfish, dense immunoreactivity was also seen in the preoptic area, which also varied seasonally and with reproductive state (Barsagade et al., 2010). The preoptic area of teleosts is well-recognized as an important node in the regulation of reproduction (Yu, Rosenblum, & Peter, 1991) and contains neurons that innervate the pituitary gland

(e.g., GnRH1 cells), which regulate hypophysiotropic functions such as gonadotropin hormone secretion (Akash et al., 2014; Zohar, Munoz-Cueto, Elizur, & Kah, 2010). In mammals, CART-immunoreactive fibers were observed in close proximity to GnRH cells in the preoptic area [Siberian hamster; (Leslie et al., 2001), and pig; (Bogus-Nowakowska et al., 2011)], and the CART-expressing neurons in the arcuate nucleus and premammillary ventral nucleus communicate with GnRH containing neurons in the POA. It is thought that this circuitry modulates GnRH1 secretion resulting in a surge of luteinizing hormone, as well as facilitating leptin's effect on GnRH secretion (Rondini, Baddini, Sousa, Bittencourt, & Elias, 2004; Subhedar, Nakhate, Upadhya, & Kokare, 2014). A recent study by True, et al. (2013) showed that CART had extensive connectivity with GnRH1 and kisspeptin-expressing neurons in the preoptic area, and electrophysiology experiments showed that CART post-synaptically depolarized both GnRH1 and kisspeptin cells (True, Verma, Grove, & Smith, 2013). In addition, CART mRNA expression and the number of CART-immunoreactive cells decreased during calorie restriction, suggesting that CART expression in animals of depressed metabolic conditions could inhibit the reproductive axis (Subhedar et al., 2014; True et al., 2013). Overall, this conserved neuroanatomical distribution from fishes to mammals suggests a potential mechanism by which nutritional status is conveyed to the reproductive system via circuitry that involves the preoptic nuclei of vertebrates.

CART-immunoreactivity is also observed in regions associated with the regulation of feeding, energy balance, and gustation in teleosts. These areas include the E, NLT, NRL, and NDIL, which all showed CART immunoreactivity in *A. burtoni*. This is consistent with previous findings that demonstrated CART-ir somata in the NLT of zebrafish and catfish (Akash et al., 2014; Subhedar et al., 2014). In zebrafish, starvation led to a reduction in *cart2*-expressing neurons of the E and NRL, and *cart4*-expressing neurons in the NLT (Akash et al., 2014). Thus, CART may have a central role in the regulation of energy balance and feeding in teleosts, similar to that described in mammals (Lin et al., 2000; Subhedar et al., 2014; Volkoff et al., 2005). Due to the whole genome duplication event in teleosts, multiple *cart* genes are reported in zebrafish (Akash et al., 2014) and in *A. burtoni* (Hu et al., 2016), and our ISH results showing divergent distributions for *cart2* and *cart4* suggest subfunctionalization. Further studies are needed to examine functional differences of these different forms.

### 4.4 | Reproductive state differences in somata size and mRNA expression

Neurons are responsible for the coordination and regulation of gene expression in response to functional needs of the organism (Ransdell, Faust, & Schulz, 2010); however, there are not always straightforward relationships between somata size, cell number, mRNA levels, and protein levels within individual neuron types. For example, a study in the European starling (*Sturnus vulgaris*) showed that changes in the number of GnRH1 and gonadotropin-inhibitory hormone (GnIH) cells throughout the breeding season, overall, mirror changes in neuronal somata size and estimated peptide concentration (Calisi, Diaz-Munoz, Wingfield, & Bentley, 2011). That study, therefore, showed a positive



relationship between cell number, cell size, and peptide concentration. In another study done in Japanese quail and domestic chickens, the authors double-labeled for NPY using IHC and ISH and demonstrated the coexistence of *npv* mRNA and NPY peptide in individual cells (Boswell, Millam, Li, & Dunn, 1998). This suggests that these cells are both transcribing *npv* mRNA as well as storing the peptide. Therefore, an increase in cell size could be due to an increase in peptide production or reduced peptide release and storage, but it is not possible to distinguish amongst these possibilities via staining techniques alone.

In our study, we tested whether neuron somata size and gene expression for candidate orexigenic and anorexigenic genes varied based on reproductive and energy consumption states. Our results showed larger NPY-ir and AGRP-ir somata in gravid compared to brooding females, and larger *pomc1a* somata in brooding compared to gravid females. One explanation for the changes in cell size between gravid and brooding females could be the need for mechanisms that allow quick adaptive changes in the neuroendocrine system without cell addition or cell death (Francis, Soma, & Fernald, 1993). For example, somata that increase in volume can support more complex dendritic inputs, which can have important functional implications for the response properties of individual neurons within the circuit (Mainen & Sejnowski, 1996; Roberts, Best, & Suter, 2006). This is potentially important in mouth brooding fish such as *A. burtoni*, as females undergo a fairly rapid transition from a gravid (energy investment) to a brooding (energy consumptive) state when her clutch of eggs is effectively transferred from her abdominal cavity into her buccal cavity during spawning. During this “motivational switch” from a self-promoting to an offspring-promoting phenotype, it is important that the neurons involved in regulating the accompanying behaviors and physiology demonstrate plasticity, especially when food intake is no longer physically possible. There is also a precedent for rapid changes in somata size in male *A. burtoni*, since GnRH1 neurons enlarge within the first 24 hr of a transition from reproductively suppressed subordinate to reproductively active dominant social status (Maruska, 2014; Maruska & Fernald, 2013). Thus, rapid changes in cell size may be a common mechanism mediating phenotypic plasticity within different neuroendocrine systems for both males and females of this species.

To further investigate the involvement of these candidate neuropeptides in the regulation of the neural control of the mouth brooding parental care strategy, including the period of necessary food deprivation, RT-qPCR was performed on macro-dissected hypothalamic tissue. We demonstrate that levels of hypothalamic *agrp* were higher in gravid compared to brooding females, which mirrors the observed differences in AGRP-ir somata sizes. The difference between reproductive states could be explained by AGRP's role as a melanocortin antagonist, and therefore, higher *agrp* mRNA levels in gravid females may contribute to regulation of the melanocortin system by inhibiting the binding of  $\alpha$ -MSH to the MC4 receptor, maintaining high food intake during the consumptive gravid phase. This is important because the females need to build up metabolic stores in addition to undergoing vitellogenesis, which would ensure that the female carries to term, and does not pre-release or cannibalize her fry. In mammals,

AGRP inhibition of POMC neurons is thought to be more important for long-term regulation of appetite than the short-term feeding behaviors typically stimulated by AGRP neuron activation (Sternson & Atasoy, 2014). Thus, AGRP neurons show bidirectional control of feeding behavior, and increased mRNA levels in gravid female *A. burtoni* may reflect changes in the maintenance of feeding during their energy investment period.

In the current study, hypothalamic mRNA levels of all other candidate genes did not differ between gravid and brooding female *A. burtoni*, and we offer several potential explanations below. First, while the females are brooding, they are physically incapable of eating so our initial prediction was that *lepr* mRNA expression would be higher during this reproductive stage, thereby increasing the sensitivity of the hypothalamus to the leptin signal to prevent the females from cannibalizing or releasing their brood. On the other hand, gravid females have to maintain their caloric intake while they undergo vitellogenesis and ovarian recrudescence, so our initial prediction was that they would have higher levels of *ghs-r1* mRNA to maintain feeding motivation and food intake. In the current study, however, mRNA levels of ghrelin receptors and leptin receptors did not differ between gravid and brooding females, so it is possible that fasting/feeding does not influence transcription, but may modify the density or turnover of receptors in certain neurons, or occur on shorter time scales (Cerde-Reverter et al., 2011). During fasting, for instance, the availability of receptors could be reduced, thereby decreasing sensitivity to hormones such as ghrelin, orexigenic neuropeptides such as NPY and AGRP, or constitutive signaling of hormones and neuropeptides.

Second, there were also no differences in hypothalamic mRNA expression of *pomc1a* and *npv* between gravid and brooding *A. burtoni* females. These results are similar to other studies that demonstrated little to no change in *pomc* hypothalamic mRNA levels associated with variations in feeding and fasting state in fishes (Cerde-Reverter et al., 2011; Sanchez, Rubio, & Cerde-Reverter, 2009). Thus, regulation of *pomc* neurons during prolonged fasting may involve other mechanisms such as differential processing of *pomc* precursors or changes in melanocortin receptor expression rather than changes in mRNA levels. Similar to our results for *npv*, a previous study in *A. burtoni* also found no differences in whole brain *npv* expression among gravid (fed), starved, and brooding (starved) females (Grone et al., 2012). Studies in other fishes show considerable variation in the response of *npv* mRNA levels to feeding conditions (Murashita, Kurokawa, Ebbesson, Stefansson, & Ronnestad, 2009; Yan et al., 2017; Yokobori et al., 2012). Thus, the regulation of *npv* mRNA may vary between species that differ in diet, digestive physiology, and metabolic trade-offs associated with life-history characteristics such as parental care. In addition, NPY is a widely distributed neuromodulator that is involved in the regulation of many other physiological processes, as well as behaviors including stress, reproduction, and aggression. Thus, investigation of potential changes in mRNA expression at finer-scale neuroanatomical resolution is needed.

Lastly, levels of *cart2* and *cart4* mRNA also did not differ between gravid and brooding *A. burtoni* females. *cart2* and *cart4* were selected

as potential candidates regulating energy balance and feeding behavior because of their previously described role in zebrafish. For example, starvation in zebrafish led to a reduction in the population of *cart2* mRNA-expressing cells of the E and NRL, and in the *cart4* mRNA-expressing cells of the NLT (Akash et al., 2014). However, our observations that hypothalamic *pomc1a* and *cart* mRNA levels do not differ between gravid and brooding females could suggest that regulation of the melanocortin receptors is primarily due to an increase in *agrp* biosynthesis rather than a decrease in *pomc1a* and *cart* biosynthesis. It is important to note, however, that mouth brooding is an extreme form of parental care and forced starvation, and there may be additional regulatory circuitry within the hypothalamus that is fundamentally different from that found in non-brooding fish species in a fasted condition. Further, in mammals, a neural circuit has been identified from the parabrachial nucleus to the central nucleus of the amygdala (CeAlc) that mediates appetite suppression during unfavorable conditions, which is different from the circuit that controls appetite suppression after feeding (Carter, Soden, Zweifel, & Palmiter, 2013). Therefore, it would be important in the future to include a starved female group (non-brooding state) with a brooding female group (unfavorable condition). Grone et al. (2012) found that food deprivation accounted for the physiological changes seen in mouth brooding females (delayed ovarian cycles and subsequent spawning, decrease in body mass), but that starvation alone did not account for the neurological changes. Thus, the starved female group (non-brooding state) could help to determine whether the conditions of the starvation state influences somata sizes and gene expression within specific brain nuclei and whether or not they are due to the parental behavioral state. In addition, it is possible that some neuromolecular mechanisms used for energy storage during the gravid phase are sufficient to support the starvation period during brooding, and are therefore not reflected in mRNA changes. Nevertheless, since these candidate neuropeptides and their functions are relatively well conserved, our work provides insights for understanding the neural control of feeding and reproductive circuits across vertebrate taxa.

## 5 | CONCLUSIONS

In this study, we provide the first complete distribution patterns of CART, NPY, and AGRP neurons throughout the entire brain of a mouth brooding teleost fish. The similarity in localization of these neuropeptides amongst teleosts, as well as with that of mammals, suggests that the neural circuitries regulating the interaction of feeding and reproduction are relatively well conserved. Reproductive- and metabolic-state plasticity in the somata size of NPY, AGRP, and *pomc1a*-expressing neurons in the *A. burtoni* brain also suggests that these neuropeptides are involved in regulating phenotypic and metabolic changes associated with the transitions between gravidity and mouth brooding parental care stages. Future studies should focus on the functional roles of these neuropeptides in regulating and maintaining reproductive and metabolic homeostasis during this transition between gravid and mouth brooding states.

## ACKNOWLEDGMENTS

We thank the reviewers and editors for helpful comments to improve the manuscript, Dr. Brian Grone for technical assistance and for providing valuable insights on the project, and members of the Maruska Lab for discussions and fish care.

## CONFLICT OF INTEREST

The authors have no known or potential conflicts of interest.

## AUTHOR CONTRIBUTIONS

All authors had full access to the data, take responsibility for the integrity of the data and accuracy of the data analysis, and approved the final manuscript. Designed experiments: KPM and DTP. Performed experiments, collected and analyzed data: DTP, DAR, and KPM. Wrote and edited the article: DTP, DAR, and KPM. Provided funding, equipment, reagents, and supplies: KPM.

## ABBREVIATIONS

4v	fourth ventricle
ac	anterior commissure
aGn	anterior glomerular nucleus
An	anterior thalamic nucleus
AP	accessory pretectal nucleus
ATn	anterior tuberal nucleus
Cc	central canal
CC	cerebellar crest
CCeG	granular layer of corpus cerebelli
CCeM	molecular layer of corpus cerebelli
CCeP	Purkinje cell layer of corpus cerebelli
CG	central gray
CM	corpus mammillare
CP	central posterior thalamic nucleus
CTn	central thalamic nucleus
CZ	central zone of tectum
DAO	dorsal accessory optic nucleus
Dc	central part of the dorsal telencephalon
Dc-1	central part of the dorsal telencephalon = subdivision 1
Dc-2	central part of the dorsal telencephalon = subdivision 2
Dc-3	central part of the dorsal telencephalon = subdivision 3
Dc-4	central part of the dorsal telencephalon = subdivision 4
Dc-5	central part of the dorsal telencephalon = subdivision 5
Dd	dorsal part of the dorsal telencephalon
Dd-d	dorsal part of the dorsal telencephalon = dorsal subdivision
DI	lateral part of the dorsal telencephalon
DI-d	dorsal part of lateral part of the dorsal telencephalon
DI-g	granular zone of lateral part of the dorsal telencephalon
DI-v1	ventral part of the lateral part of the dorsal telencephalon = subdivision 1
DI-v2	ventral part of the lateral part of the dorsal telencephalon = subdivision 2

Dm	medial part of the dorsal telencephalon	NLTv	lateral tuberal nucleus = ventral part
Dm-1	medial part of the dorsal telencephalon = subdivision 1	NLVa	anterior part of nucleus of the lateral valvulae
Dm-2c	medial part of the dorsal telencephalon = caudal subdivision 2	NLVc	central part of nucleus of the lateral valvulae
Dm-2r	medial part of the dorsal telencephalon = rostral subdivision 2	NMIL	medial nucleus of the interior lobe
Dm-3	medial part of the dorsal telencephalon = subdivision 3	nMLF	nucleus of medial longitudinal fasciculus
DON	descending octavolateralis nucleus	nMMP	magnocellular preoptic nucleus = magnocellular division
Dp	posterior part of the dorsal telencephalon	NP	nucleus pretectalis
DP	dorsal posterior thalamic nucleus	NPC	central pretectal nucleus
dt	descending trigeminal tract	nPPa	parvocellular preoptic nucleus = anterior part
DT	dorsal tegmental nucleus	nPMP	magnocellular preoptic nucleus = parvocellular division
DWZ	deep white zone of tectum	nPPp	parvocellular preoptic nucleus = posterior part
Dx	unassigned subdivision of dorsal telencephalon	NPT	posterior tuberal nucleus
E	entopeduncular nucleus	NR	nucleus ruber
ECL	external cell layer of olfactory bulb	NRL	nucleus of the lateral recess
EG	granular eminence	NRP	nucleus of the posterior recess
fr	fasciculus retroflexus	NT	nucleus taenia
GL	glomerular layer of olfactory bulb	nTE	nucleus of the thalamic eminentia
Gn	glomerular nucleus	OEN	octavolateralis efferent nucleus
gTN	ganglion of the terminal nerve	ON	optic nerve
hc	horizontal commissure	PAG	periaqueductal gray
IC	intercalated nucleus	pc	posterior commissure
ICL	inner cell layer of olfactory bulb	PGc	commissural preglomerular nucleus
ICo	isthmus commissure	PGm	medial preglomerular nucleus
IIIn	oculomotor nucleus	PGn	preglomerular nucleus
IO	inferior olive	Pgd	dorsal preglomerular nucleus
IP	interpeduncular nucleus	PGl	lateral preglomerular nucleus
IVn	trochlear nucleus	PGm	medial preglomerular nucleus
LC	locus coeruleus	PGZ	periventricular gray zone of tectum
LFB	lateral forebrain bundle	Pit	pituitary
LFN	lateral funicular nucleus	PLm	medial part of the perilemniscular nucleus
LL	lateral lemniscus	PN	prethalamic nucleus
LT	lateral tegmental nucleus	PPd	dorsal periventricular pretectal nucleus
MFN	medial funicular nucleus	PPv	ventral part of the periventricular pretectal nucleus
mlf	medial longitudinal fasciculus	PS	pineal stalk
MON	medial octavolateralis nucleus	PSi	superficial pretectal nucleus = intermediate division
NC	nucleus corticalis	PSm	superficial pretectal nucleus = medial division
NCIL	central nucleus of the inferior lobe	PSP	parvocellular superficial pretectal nucleus
NDILc	caudal part of the diffuse nucleus of the inferior lobe	PT	posterior thalamic nucleus
NDILl	lateral part of the diffuse nucleus of the inferior lobe	PTN	posterior tuberal nucleus
NDILm	medial part of the diffuse nucleus of the inferior lobe	PTT	paratoral tegmental nucleus
nGMp	magnocellular preoptic nucleus = gigantocellular division	PVO	paraventricular organ
nHd	dorsal habenular nucleus	Ri	inferior reticular nucleus
nHv	ventral habenular nucleus	Rm	medial reticular nucleus
NI	nucleus isthmi	Rs	superior reticular formation
NLL	nucleus of the lateral lemniscus	SGn	secondary gustatory nucleus
NLT	lateral tuberal nucleus	sgt	secondary gustatory tract
NLTd	lateral tuberal nucleus = dorsal part	SOF	secondary olfactory layer of olfactory bulb
NLTi	lateral tuberal nucleus = intermediate part	SR	superior raphe nucleus
NLTl	lateral tuberal nucleus = lateral part	SVn	secondary visceral nucleus
NLTm	lateral tuberal nucleus = medial part	SWGZ	superficial gray and white zone of tectum
		T	tectum
		TBT	tectobulbar tract



TGN	tertiary gustatory nucleus
TL	torus longitudinalis
TLa	torus lateralis
TMCa	anterior mesencephalocerebellar tract
TMCp	posterior mesencephalocerebellar tract
TPp	periventricular nucleus of posterior tuberculum
TS	torus semicircularis
TSc	central nucleus of torus semicircularis
TSvl	ventrolateral nucleus of torus semicircularis
VAO	ventral accessory optic nucleus
Vc	central part of the ventral telencephalon
VCeG	granular layer of valvula cerebelli
VCeM	molecular layer of valvula cerebelli
VCeP	Purkinje layer of valvula cerebelli
Vd	dorsal part of the ventral telencephalon
Vd-c	dorsal part of the ventral telencephalon = caudal subdivision
Vd-r	dorsal part of the ventral telencephalon = rostral subdivision
Vde	descending tract of the trigeminal nerve
VH	ventral horn
Vi	intermediate nucleus of the ventral telencephalon
VI	lateral part of the ventral telencephalon
VL	Vagal lobe
VLn	ventrolateral thalamic nucleus
Vllm	facial motor nucleus
Vlls	facial sensory nucleus
VMn	ventromedial thalamic nucleus
VOT	ventral optic tract
Vp	postcommissural nucleus of the ventral telencephalon
Vs	supracommissural nucleus of the ventral telencephalon
Vs-l	lateral part of the supracommissural nucleus of the ventral telencephalon
Vs-m	medial part of the supracommissural nucleus of the ventral telencephalon
Vv	ventral nucleus of the ventral telencephalon
Xm	vagal motor nucleus

## REFERENCES

- Agulleiro, M. J., Cortes, R., Leal, E., Rios, D., Sanchez, E., & Cerda-Reverter, J. M. (2014). Characterization, tissue distribution and regulation by fasting of the agouti family of peptides in the sea bass (*Dicentrarchus labrax*). [Research Support, Non-U.S. Gov't]. *General and Comparative Endocrinology*, 205, 251–259. doi: 10.1016/j.ygcen.2014.02.009
- Akash, G., Kaniganti, T., Tiwari, N. K., Subhedar, N. K., & Ghose, A. (2014). Differential distribution and energy status-dependent regulation of the four CART neuropeptide genes in the zebrafish brain. [Research Support, Non-U.S. Gov't]. *Journal of Comparative Neurology*, 522(10), 2266–2285. doi: 10.1002/cne.23532
- Amano, M., Takahashi, A., Yamanome, T., Oka, Y., Amiya, N., Kawauchi, H., & Yamamori, K. (2005). Immunocytochemical localization and ontogenic development of alpha-melanocyte-stimulating hormone (alpha-MSH) in the brain of a pleuronectiform fish, barfin flounder. [Research Support, Non-U.S. Gov't]. *Cell and Tissue Research*, 320(1), 127–134. doi: 10.1007/s00441-004-1058-4
- Barsagade, V. G., Mazumdar, M., Singru, P. S., Thim, L., Clausen, J. T., & Subhedar, N. (2010). Reproductive phase-related variations in cocaine- and amphetamine-regulated transcript (CART) in the olfactory system, forebrain, and pituitary of the female catfish, *Clarias batrachus* (Linn.). [Research Support, Non-U.S. Gov't]. *Journal of Comparative Neurology*, 518(13), 2503–2524. doi: 10.1002/cne.22349
- Batten, T. F., Cambre, M. L., Moons, L., & Vandesande, F. (1990). Comparative distribution of neuropeptide-immunoreactive systems in the brain of the green molly, *Poecilia latipinna*. *Journal of Comparative Neurology*, 302(4), 893–919.
- Bogus-Nowakowska, K., Robak, A., Rowniak, M., Wasilewska, B., Najdzion, J., Kolenkiewicz, M., ... Majewski, M. (2011). Distribution and chemical coding pattern of the cocaine- and amphetamine-regulated transcript (CART) immunoreactivity in the preoptic area of the pig. *Folia Histochemica et Cytobiologica*, 49(4), 604–614.
- Boswell, T., Millam, J. R., Li, Q., & Dunn, I. C. (1998). Cellular localization of neuropeptide Y mRNA and peptide in the brain of the Japanese quail and domestic chicken. [Comparative Study Research Support, Non-U.S. Gov't]. *Cell and Tissue Research*, 293(1), 31–38.
- Burmeister, S. S., Munshi, R. G., & Fernald, R. D. (2009). Cytoarchitecture of a cichlid fish telencephalon. *Brain, Behavior and Evolution*, 74(2), 110–120. doi: 000235613 [pii]
- Bustin, S. A., Benes, V., Nolan, T., & Pfaffl, M. W. (2005). Quantitative real-time RT-PCR—a perspective. *Journal of Molecular Endocrinology*, 34(3), 597–601. doi: 34/3/597 [pii] [PMC][10.1677/jme.1.01755] 10.1677/jme.1.01755
- Butler, J. M., & Maruska, K. P. (2016). The mechanosensory lateral line system mediates activation of socially-relevant brain regions during territorial interactions. *Frontiers in Behavioral Neuroscience*, 10, 93. doi: 10.3389/fnbeh.2016.00093
- Calisi, R. M., Diaz-Munoz, S. L., Wingfield, J. C., & Bentley, G. E. (2011). Social and breeding status are associated with the expression of GnIH. [Research Support, Non-U.S. Gov't Research Support, U.S. Gov't, Non-P.H.S.]. *Genes, Brain and Behavior*, 10(5), 557–564. doi: 10.1111/j.1601-183X.2011.00693.x
- Carter, M. E., Soden, M. E., Zweifel, L. S., & Palmiter, R. D. (2013). Genetic identification of a neural circuit that suppresses appetite. [Research Support, N.I.H., Extramural Research Support, Non-U.S. Gov't]. *Nature*, 503(7474), 111–114. doi: 10.1038/nature12596
- Cerda-Reverter, J. M., Agulleiro, M. J., Raul Guillot, R. G., Sanchez, E., Ceinos, R., & Rotllant, J. (2011). Fish melanocortin system. [Research Support, Non-U.S. Gov't Review]. *European Journal of Pharmacology*, 660(1), 53–60. doi: 10.1016/j.ejphar.2010.10.108
- Cerda-Reverter, J. M., Anglade, I., Martinez-Rodriguez, G., Mazurais, D., Munoz-Cueto, J. A., Carrillo, M., ... Zanuy, S. (2000). Characterization of neuropeptide Y expression in the brain of a perciform fish, the sea bass (*Dicentrarchus labrax*). *Journal of Chemical Neuroanatomy*, 19(4), 197–210.
- Cerda-Reverter, J. M., & Peter, R. E. (2003). Endogenous melanocortin antagonist in fish: structure, brain mapping, and regulation by fasting of the goldfish agouti-related protein gene. [Research Support, Non-U.S. Gov't]. *Endocrinology*, 144(10), 4552–4561. doi: 10.1210/en.2003-0453
- Chiba, A., Oka, S., & Honma, Y. (1996). Ontogenetic changes in neuropeptide Y-like-immunoreactivity in the terminal nerve of the chum salmon and the cloudy dogfish, with special reference to colocalization with gonadotropin-releasing hormone-immunoreactivity. *Neuroscience Letters*, 213(1), 49–52. doi: 0304394096128287 [pii]
- Clutton-Brock, T. H., & Vincent, A. C. (1991). Sexual selection and the potential reproductive rates of males and females. [Comparative Study]. *Nature*, 351(6321), 58–60. doi: 10.1038/351058a0

- Copeland, D. L., Duff, R. J., Liu, Q., Prokop, J., & Londraville, R. L. (2011). Leptin in teleost fishes: An argument for comparative study. *Frontiers in Physiology*, 2, 26. doi: 10.3389/fphys.2011.00026
- Couceyro, P. R., Koylu, E. O., & Kuhar, M. J. (1997). Further studies on the anatomical distribution of CART by in situ hybridization. [Research Support, Non-U.S. Gov't Research Support, U.S. Gov't, P. H.S.]. *Journal of Chemical Neuroanatomy*, 12(4), 229–241.
- Danger, J. M., Breton, B., Vallarino, M., Fournier, A., Pelletier, G., & Vaudry, H. (1991). Neuropeptide-Y in the trout brain and pituitary: Localization, characterization, and action on gonadotropin release. [Research Support, Non-U.S. Gov't]. *Endocrinology*, 128(5), 2360–2368. doi: 10.1210/endo-128-5-2360
- Daniel, J. A., Foradori, C. D., Whitlock, B. K., & Sartin, J. L. (2013). Hypothalamic integration of nutrient status and reproduction in the sheep. [Review]. *Reproduction in Domestic Animals*, 48 Suppl 1, 44–52. doi: 10.1111/rda.12227
- Fernald, R. D., & Hirata, N. R. (1979). The ontogeny of social behavior and body coloration in the African cichlid fish *Haplochromis burtoni*. *Zeitschrift für Tierpsychologie*, 50, 180–187.
- Forlano, P. M., & Cone, R. D. (2007). Conserved neurochemical pathways involved in hypothalamic control of energy homeostasis. [Research Support, N.I.H., Extramural Research Support, Non-U.S. Gov't]. *Journal of Comparative Neurology*, 505(3), 235–248. doi: 10.1002/cne.21447
- Francis, R. C., Soma, K., & Fernald, R. D. (1993). Social regulation of the brain-pituitary-gonadal axis. *Proceedings of the National Academy of Sciences of the United States of America*, 90, 7794–7798.
- Gaikwad, A., Biju, K. C., Saha, S. G., & Subhedar, N. (2004). Neuropeptide Y in the olfactory system, forebrain and pituitary of the teleost, *Clarias batrachus*. *Journal of Chemical Neuroanatomy*, 27(1), 55–70.
- Grone, B. P., Carpenter, R. E., Lee, M., Maruska, K. P., & Fernald, R. D. (2012). Food deprivation explains effects of mouthbrooding on ovaries and steroid hormones, but not brain neuropeptide and receptor mRNAs, in an African cichlid fish. *Hormones and Behavior*, 62(1), 18–26. doi: S0018-506X(12)00130-4
- Grone, B. P., & Maruska, K. P. (2015). A second corticotropin-releasing hormone gene (CRH2) is conserved across vertebrate classes and expressed in the hindbrain of a basal neopterygian fish, the spotted gar (*Lepisosteus oculatus*). [Research Support, Non-U.S. Gov't]. *Journal of Comparative Neurology*, 523(7), 1125–1143. doi: 10.1002/cne.23729
- Harris, R. M., Dijkstra, P. D., & Hofmann, H. A. (2014). Complex structural and regulatory evolution of the pro-opiomelanocortin gene family. [Comparative Study Research Support, Non-U.S. Gov't]. *General and Comparative Endocrinology*, 195, 107–115. doi: 10.1016/j.ygcen.2013.10.007
- Hoskins, L. J., & Volkoff, H. (2012). The comparative endocrinology of feeding in fish: Insights and challenges. [Research Support, Non-U.S. Gov't Review]. *General and Comparative Endocrinology*, 176(3), 327–335. doi: 10.1016/j.ygcen.2011.12.025
- Hu, C. K., Southey, B. R., Romanova, E. V., Maruska, K. P., Sweedler, J. V., & Fernald, R. D. (2016). Identification of prohormones and pituitary neuropeptides in the African cichlid, *Astatotilapia burtoni*. *BMC Genomics*, 17(1), 660. doi: 10.1186/s12864-016-2914-9
- Imura, K., Yamamoto, N., Sawai, N., Yoshimoto, M., Yang, C. Y., Xue, H. G., & Ito, H. (2003). Topographical organization of an indirect telencephalo-cerebellar pathway through the nucleus paracommissuralis in a teleost, *Oreochromis niloticus*. *Brain, Behavior and Evolution*, 61(2), 70–90.
- Kah, O., Pontet, A., Danger, J. M., Dubourg, P., Pelletier, G., Vaudry, H., & Calas, A. (1989). Characterization, cerebral distribution and gonadotropin release activity of neuropeptide Y (NPY) in the goldfish. *Fish Physiology and Biochemistry*, 7(1–6), 69–76. doi: 10.1007/BF00004691
- Kong, D., Tong, Q., Ye, C., Koda, S., Fuller, P. M., Krashes, M. J., ... Lowell, B. B. (2012). GABAergic RIP-Cre neurons in the arcuate nucleus selectively regulate energy expenditure. [Research Support, N.I.H., Extramural Research Support, Non-U.S. Gov't]. *Cell*, 151(3), 645–657. doi: 10.1016/j.cell.2012.09.020
- Koylu, E. O., Couceyro, P. R., Lambert, P. D., & Kuhar, M. J. (1998). Cocaine- and amphetamine-regulated transcript peptide immunohistochemical localization in the rat brain. [Research Support, U.S. Gov't, P.H.S.]. *Journal of Comparative Neurology*, 391(1), 115–132.
- Lazar, G., Calle, M., Roubos, E. W., & Kozicz, T. (2004). Immunohistochemical localization of cocaine- and amphetamine-regulated transcript peptide in the central nervous system of the frog *Rana esculenta*. [Comparative Study Research Support, Non-U.S. Gov't]. *Journal of Comparative Neurology*, 477(3), 324–339. doi: 10.1002/cne.20264
- Leslie, R. A., Sanders, S. J., Anderson, S. I., Schuhler, S., Horan, T. L., & Ebling, F. J. (2001). Appositions between cocaine and amphetamine-related transcript- and gonadotropin releasing hormone-immunoreactive neurons in the hypothalamus of the Siberian hamster. [Research Support, Non-U.S. Gov't]. *Neuroscience Letters*, 314(3), 111–114.
- Lin, X., Volkoff, H., Narnaware, Y., Bernier, N. J., Peyon, P., & Peter, R. E. (2000). Brain regulation of feeding behavior and food intake in fish. [Research Support, Non-U.S. Gov't Review]. *Comparative Biochemistry and Physiology Part A: Molecular & Integrative Physiology*, 126(4), 415–434.
- Liu, Q., Chen, Y., Copeland, D., Ball, H., Duff, R. J., Rockich, B., & Londraville, R. L. (2010). Expression of leptin receptor gene in developing and adult zebrafish. [Comparative Study Research Support, N.I.H., Extramural]. *General and Comparative Endocrinology*, 166(2), 346–355. doi: 10.1016/j.ygcen.2009.11.015
- Mainen, Z. F., & Sejnowski, T. J. (1996). Influence of dendritic structure on firing pattern in model neocortical neurons. [Research Support, Non-U.S. Gov't]. *Nature*, 382(6589), 363–366. doi: 10.1038/382363a0
- Marchetti, G., Cozzi, B., Tavanti, M., Russo, V., Pellegrini, S., & Fabiani, O. (2000). The distribution of neuropeptide Y-immunoreactive neurons and nerve fibers in the forebrain of the carp *Cyprinus carpio* L. *Journal of Chemical Neuroanatomy*, 20(2), 129–139.
- Maruska, K. P. (2014). Social regulation of reproduction in male cichlid fishes. [Research Support, Non-U.S. Gov't]. *General and Comparative Endocrinology*, 207, 2–12. doi: 10.1016/j.ygcen.2014.04.038
- Maruska, K. P., Becker, L., Neboori, A., & Fernald, R. D. (2013). Social descent with territory loss causes rapid behavioral, endocrine, and transcriptional changes in the brain. *Journal of Experimental Biology*, 216, 3656–3666. doi: 10.1242/jeb.088617
- Maruska, K. P., Butler, J. M., Field, K. E., & Porter, D. T. (2017). Localization of glutamatergic, GABAergic, and cholinergic neurons in the brain of the African cichlid fish, *Astatotilapia burtoni*. *Journal of Comparative Neurology*, 525(3), 610–638. doi: 10.1002/cne.24092
- Maruska, K. P., & Fernald, R. D. (2013). Social regulation of male reproductive plasticity in an African cichlid fish. *Integrative and Comparative Biology*, 207, 2–12. doi: 10.1093/icb/ict017
- Maruska, K. P., Levavi-Sivan, B., Biran, J., & Fernald, R. D. (2011). Plasticity of the reproductive axis caused by social status change in an African cichlid fish: I. pituitary gonadotropins. *Endocrinology*, 152, 281–290.
- Maruska, K. P., Zhang, A., Neboori, A., & Fernald, R. D. (2013). Social opportunity causes rapid transcriptional changes in the social behavior network of the brain in an African cichlid fish. *Journal of Neuroendocrinology*, 25, 145–157.
- Mitter, K., Kotoulas, G., Magoulas, A., Mulero, V., Sepulcre, P., Figueras, A., ... Sarropoulou, E. (2009). Evaluation of candidate reference genes for

- QPCR during ontogenesis and of immune-relevant tissues of European seabass (*Dicentrarchus labrax*). *Comparative Biochemistry and Physiology Part B: Biochemistry and Molecular Biology*, 153(4), 340–347. doi: 10.1096-4959(09)00109-2 [pii] 10.1016/j.cbpb.2009.04.009
- Mousley, A., Polese, G., Marks, N. J., & Eisthen, H. L. (2006). Terminal nerve-derived neuropeptide  $\gamma$  modulates physiological responses in the olfactory epithelium of hungry axolotls (*Ambystoma mexicanum*). [Research Support, N.I.H., Extramural Research Support, Non-U.S. Gov't]. *Journal of Neuroscience*, 26(29), 7707–7717. doi: 10.1523/JNEUROSCI.1977-06.2006
- Mukherjee, A., Subhedar, N. K., & Ghose, A. (2012). Ontogeny of the cocaine- and amphetamine-regulated transcript (CART) neuropeptide system in the brain of zebrafish, *Danio rerio*. [Research Support, Non-U.S. Gov't]. *Journal of Comparative Neurology*, 520(4), 770–797. doi: 10.1002/cne.22779
- Munchrath, L. A., & Hofmann, H. A. (2010). Distribution of sex steroid hormone receptors in the brain of an African cichlid fish, *Astatotilapia burtoni*. *Journal of Comparative Neurology*, 518(16), 3302–3326. doi: 10.1002/cne.22401
- Munoz-Cueto, J. A., Sarasquete, C., Zohar, A. H., & Kah, O. (2001). *An atlas of the brain of the gilthead seabream (Sparus aurata)*. College Park: Maryland Sea Grant.
- Murashita, K., Kurokawa, T., Ebbesson, L. O., Stefansson, S. O., & Ronnestad, I. (2009). Characterization, tissue distribution, and regulation of agouti-related protein (AgRP), cocaine- and amphetamine-regulated transcript (CART) and neuropeptide Y (NPY) in Atlantic salmon (*Salmo salar*). [Research Support, Non-U.S. Gov't]. *General and Comparative Endocrinology*, 162(2), 160–171. doi: 10.1016/j.ygcen.2009.03.015
- Nakagawa, S. (2004). A farewell to Bonferroni: The problems of low statistical power and publication bias. *Behavioral Ecology*, 15(6), 1044–1045.
- Navarro, V. M., & Kaiser, U. B. (2013). Metabolic influences on neuroendocrine regulation of reproduction. [Research Support, N.I.H., Extramural Review]. *Current Opinion in Endocrinology, Diabetes and Obesity*, 20(4), 335–341. doi: 10.1097/MED.0b013e32832836318ce
- O'Connell, L. A., & Hofmann, H. A. (2011). The vertebrate mesolimbic reward system and social behavior network: A comparative synthesis. *Journal of Comparative Neurology*, 519, 3599–3639. doi: 10.1002/cne.22735
- Pickavance, L. C., Staines, W. A., & Fryer, J. N. (1992). Distributions and colocalization of neuropeptide Y and somatostatin in the goldfish brain. [Research Support, Non-U.S. Gov't]. *Journal of Chemical Neuroanatomy*, 5(3), 221–233.
- Pontet, A., Danger, J. M., Dubourg, P., Pelletier, G., Vaudry, H., Calas, A., & Kah, O. (1989). Distribution and characterization of neuropeptide Y-like immunoreactivity in the brain and pituitary of the goldfish. *Cell and Tissue Research*, 255(3), 529–538.
- Ransdell, J. L., Faust, T. B., & Schulz, D. J. (2010). Correlated levels of mRNA and soma size in single identified neurons: Evidence for compartment-specific regulation of gene expression. *Frontiers in Molecular Neuroscience*, 3, 116. doi: 10.3389/fnmol.2010.00116
- Reiner, A., & Northcutt, R. G. (1992). An immunohistochemical study of the telencephalon of the senegal bichir (*Polypterus senegalus*). [Research Support, U.S. Gov't, P.H.S.]. *Journal of Comparative Neurology*, 319(3), 359–386. doi: 10.1002/cne.903190305
- Renn, S. C., Carleton, J. B., Magee, H., Nguyen, M. L., & Tanner, A. C. (2009). Maternal care and altered social phenotype in a recently collected stock of *Astatotilapia burtoni* cichlid fish. *Integrative and Comparative Biology*, 49(6), 660–673. doi: 10.1093/icb/49(6)660 [pii] 10.1093/icb/49(6)660
- Ringholm, A., Klovins, J., Fredriksson, R., Poliakova, N., Larson, E. T., Kukkonen, J. P., ... Schioth, H. B. (2003). Presence of melanocortin (MC4) receptor in spiny dogfish suggests an ancient vertebrate origin of central melanocortin system. [Research Support, Non-U.S. Gov't]. *European Journal of Biochemistry*, 270(2), 213–221.
- Roa, J. (2013). Role of GnRH neurons and their neuronal afferents as key integrators between food intake regulatory signals and the control of reproduction. [Review]. *International Journal of Endocrinology*, 2013, 518046. doi: 10.1155/2013/518046
- Roberts, C. B., Best, J. A., & Suter, K. J. (2006). Dendritic processing of excitatory synaptic input in hypothalamic gonadotropin releasing-hormone neurons. [Research Support, N.I.H., Extramural]. *Endocrinology*, 147(3), 1545–1555. doi: 10.1210/en.2005-1350
- Rodriguez-Gomez, F. J., Rendon-Unceta, C., Sarasquete, C., & Munoz-Cueto, J. A. (2001). Distribution of neuropeptide Y-like immunoreactivity in the brain of the Senegalese sole (*Solea senegalensis*). [Research Support, Non-U.S. Gov't]. *Anatomical Record*, 262(3), 227–237.
- Rondini, T. A., Baddini, S. P., Sousa, L. F., Bittencourt, J. C., & Elias, C. F. (2004). Hypothalamic cocaine- and amphetamine-regulated transcript neurons project to areas expressing gonadotropin releasing hormone immunoreactivity and to the anteroventral periventricular nucleus in male and female rats. [Research Support, Non-U.S. Gov't]. *Neuroscience*, 125(3), 735–748. doi: 10.1016/j.neuroscience.2003.12.045
- Sakharkar, A. J., Singru, P. S., Sarkar, K., & Subhedar, N. K. (2005). Neuropeptide Y in the forebrain of the adult male cichlid fish *Oreochromis mossambicus*: Distribution, effects of castration and testosterone replacement. *Journal of Comparative Neurology*, 489(2), 148–165.
- Sanchez, E., Rubio, V. C., & Cerda-Reverter, J. M. (2009). Characterization of the sea bass melanocortin 5 receptor: A putative role in hepatic lipid metabolism. [Research Support, Non-U.S. Gov't]. *Journal of Experimental Biology*, 212(Pt 23), 3901–3910. doi: 10.1242/jeb.035121
- Schioth, H. B., & Watanobe, H. (2002). Melanocortins and reproduction. [Research Support, Non-U.S. Gov't Review]. *Brain Research. Brain Research Reviews*, 38(3), 340–350.
- Schneider, J. E. (2004). Energy balance and reproduction. [Research Support, U.S. Gov't, Non-P.H.S. Review]. *Physiology & Behavior*, 81(2), 289–317. doi: 10.1016/j.physbeh.2004.02.007
- Shahjahan, M., Kitahashi, T., & Parhar, I. S. (2014). Central pathways integrating metabolism and reproduction in teleosts. [Review]. *Frontiers in Endocrinology (Lausanne)*, 5, 36. doi: 10.3389/fendo.2014.00036
- Singru, P. S., Mazumdar, M., Sakharkar, A. J., Lechan, R. M., Thim, L., Clausen, J. T., & Subhedar, N. K. (2007). Immunohistochemical localization of cocaine- and amphetamine-regulated transcript peptide in the brain of the catfish, *Clarias batrachus* (Linn.). *Journal of Comparative Neurology*, 502(2), 215–235.
- Sohn, J. W., Elmquist, J. K., & Williams, K. W. (2013). Neuronal circuits that regulate feeding behavior and metabolism. [Research Support, N.I.H., Extramural Research Support, Non-U.S. Gov't Review]. *Trends in Neurosciences*, 36(9), 504–512. doi: 10.1016/j.tins.2013.05.003
- Song, Y., Golling, G., Thacker, T. L., & Cone, R. D. (2003). Agouti-related protein (AGRP) is conserved and regulated by metabolic state in the zebrafish, *Danio rerio*. [Research Support, Non-U.S. Gov't]. *Endocrine*, 22(3), 257–265. doi: 10.1385/ENDO:22:3:257
- Sternson, S. M., & Atasoy, D. (2014). Agouti-related protein neuron circuits that regulate appetite. [Review]. *Neuroendocrinology*, 100(2–3), 95–102. doi: 10.1159/000369072
- Subhedar, N., Cerda, J., & Wallace, R. A. (1996). Neuropeptide Y in the forebrain and retina of the killifish, *Fundulus heteroclitus*. [Research Support, Non-U.S. Gov't Research Support, U.S. Gov't, Non-P.H.S.]. *Cell and Tissue Research*, 283(2), 313–323.
- Subhedar, N. K., Nakhate, K. T., Upadhya, M. A., & Kokare, D. M. (2014). CART in the brain of vertebrates: Circuits, functions and evolution.



- [Research Support, Non-U.S. Gov't Review]. *Peptides*, 54, 108–130. doi: 10.1016/j.peptides.2014.01.004
- Tena-Sempere, M. (2007). Roles of ghrelin and leptin in the control of reproductive function. [Research Support, Non-U.S. Gov't]. *Neuroendocrinology*, 86(3), 229–241. doi: 10.1159/000108410
- True, C., Verma, S., Grove, K. L., & Smith, M. S. (2013). Cocaine- and amphetamine-regulated transcript is a potent stimulator of GnRH and kisspeptin cells and may contribute to negative energy balance-induced reproductive inhibition in females. [Research Support, N.I.H., Extramural Research Support, Non-U.S. Gov't]. *Endocrinology*, 154(8), 2821–2832. doi: 10.1210/en.2013-1156
- Volkoff, H., Canosa, L. F., Unniappan, S., Cerda-Reverter, J. M., Bernier, N. J., Kelly, S. P., & Peter, R. E. (2005). Neuropeptides and the control of food intake in fish. [Research Support, Non-U.S. Gov't Review]. *General and Comparative Endocrinology*, 142(1–2), 3–19. doi: 10.1016/j.ygcen.2004.11.001
- Wade, G. N., & Jones, J. E. (2004). Neuroendocrinology of nutritional infertility. [Research Support, U.S. Gov't, P.H.S. Review]. *American Journal of Physiology. Regulatory, Integrative and Comparative Physiology*, 287(6), R1277–R1296. doi: 10.1152/ajpregu.00475.2004
- Wan, Y., Zhang, Y., Ji, P., Li, Y., Xu, P., & Sun, X. (2012). Molecular characterization of CART, AgRP, and MC4R genes and their expression with fasting and re-feeding in common carp (*Cyprinus carpio*). [Comparative Study Research Support, Non-U.S. Gov't]. *Molecular Biology Reports*, 39(3), 2215–2223. doi: 10.1007/s11033-011-0970-4
- Williams, K. W., & Elmquist, J. K. (2012). From neuroanatomy to behavior: Central integration of peripheral signals regulating feeding behavior. [Research Support, N.I.H., Extramural Research Support, Non-U.S. Gov't Review]. *Nature Neuroscience*, 15(10), 1350–1355. doi: 10.1038/nn.3217
- Wullimann, M. F., Rupp, B., & Reichert, H. (1996). *Neuroanatomy of the zebrafish brain: A topological atlas*. Basel: Birkhauser Verlag.
- Yan, P., Jia, J., Yang, G., Wang, D., Sun, C., & Li, W. (2017). Duplication of neuropeptide Y and peptide YY in Nile tilapia *Oreochromis niloticus* and their roles in food intake regulation. *Peptides*, 88, 97–105. doi: 10.1016/j.peptides.2016.12.010
- Yang, Y., Atasoy, D., Su, H. H., & Sternson, S. M. (2011). Hunger states switch a flip-flop memory circuit via a synaptic AMPK-dependent positive feedback loop. [Research Support, Non-U.S. Gov't]. *Cell*, 146(6), 992–1003. doi: 10.1016/j.cell.2011.07.039
- Yokobori, E., Azuma, M., Nishiguchi, R., Kang, K. S., Kamijo, M., Uchiyama, M., & Matsuda, K. (2012). Neuropeptide Y stimulates food intake in the Zebrafish, *Danio rerio*. [Research Support, Non-U.S. Gov't]. *Journal of Neuroendocrinology*, 24(5), 766–773. doi: 10.1111/j.1365-2826.2012.02281.x
- Yu, K. L., Rosenblum, P. M., & Peter, R. E. (1991). In vitro release of gonadotropin-releasing hormone from the brain preoptic-anterior hypothalamic region and pituitary of female goldfish. [Research Support, Non-U.S. Gov't]. *General and Comparative Endocrinology*, 81(2), 256–267.
- Zahid, M., Malik, S., & Rani, S. (2014). Neuropeptide Y (NPY) distribution in the forebrain of adult spiny eel, *Macrognathus pancalus*. *Journal of Endocrinology*, 2, 75–86.
- Zhang, C., Forlano, P. M., & Cone, R. D. (2012). AgRP and POMC neurons are hypophysiotropic and coordinately regulate multiple endocrine axes in a larval teleost. [Research Support, N.I.H., Extramural]. *Cell Metabolism*, 15(2), 256–264. doi: 10.1016/j.cmet.2011.12.014
- Zhao, S., & Fernald, R. D. (2005). Comprehensive algorithm for quantitative real-time polymerase chain reaction. *Journal of Computational Biology*, 12(8), 1047–1064.
- Zohar, Y., Munoz-Cueto, J. A., Elizur, A., & Kah, O. (2010). Neuroendocrinology of reproduction in teleost fish. [Review]. *General and Comparative Endocrinology*, 165(3), 438–455. doi: 10.1016/j.ygcen.2009.04.017

**How to cite this article:** Porter DT, Roberts DA, Maruska KP. Distribution and female reproductive state differences in orexigenic and anorexigenic neurons in the brain of the mouth brooding African cichlid fish, *Astatotilapia burtoni*. *J Comp Neurol*. 2017;525:3126–3157. <https://doi.org/10.1002/cne.24268>